Journal of Natural Gas Science and Engineering 84 (2020) 103629

Contents lists available at ScienceDirect

Journal of Natural Gas Science and Engineering

journal homepage: http://www.elsevier.com/locate/jngse

# Characteristics of gas chimneys and their implications on gas hydrate accumulation in the Shenhu area, northern south China sea

Cong Cheng [a,b], Tao Jiang [a,b,*], Zenggui Kuang [b,c,d], Chengzhi Yang [b,c,d,**], Cheng Zhang [a], Yunlong He [a], Zhen Cheng [a], Dongmei Tian [a], Pengfei Xiong [a]

[a] Hubei Key Laboratory of Marine Geological Resources, China University of Geosciences, Wuhan, 430074, China
[b] Southern Marine Science and Engineering Guangdong Laboratory (Guangzhou), Guangzhou, 511458, China
[c] Gas Hydrate Engineering and Technology Center, Guangzhou Marine Geological Survey, Guangzhou, 510075, China
[d] MNR Key Laboratory of Marine Mineral Resources, Guangzhou Marine Geological Survey, Guangzhou, 510075, China

ARTICLE INFO

*Keywords:*
Gas chimney
Gas hydrate
Gas migration pathways
Gas hydrate accumulation
Shenhu area

ABSTRACT

Gas hydrates have captivated extensive concentration from scholars all over the world as potential alternative energy sources. In 2017, the Guangzhou Marine Geological Survey (GMGS) carried out a successful gas hydrate production test in the Shenhu area, which was of considerable significance to the study of gas hydrates in China. Several studies describing gas chimneys as the primary vertical gas migration pathways in the Shenhu area were mainly based on two-dimensional (2D) seismic data. In this research, on the basis of high-resolution three-dimensional (3D) seismic data newly acquired in 2018, combined with well logging data acquired during the 2007 and 2015 expeditions, the contribution of gas chimneys to gas hydrate accumulation was determined. As a result, four types of gas chimneys with various top shapes were identified, and their internal seismic reflection characteristics were predominantly chaotic, acoustic blanking, and high-amplitude reflection from bottom to top. Moreover, thick hydrate layers were discovered above some of the gas chimneys. Further analyses on the hydrocarbon generation and tectono-sedimentary evolution in the Baiyun Sag indicated the evolution of gas chimneys could be divided into five stages. Furthermore, as the primary vertical gas migration pathways in the Shenhu area, gas chimneys could be sourced from the Wenchang formation and Enping formation and could pierce into the Quaternary gas hydrate reservoirs. This resulted in deep thermogenic gas directly migrating upward into the gas hydrate stability zone (GHSZ) and accumulating into thick hydrate layers on or above the top of gas chimneys.

## 1. Introduction

Gas hydrates are ice-like solid compounds compounded by the combination of water and gas, such as methane and ethane, at high-pressure and low temperatures conditions. They usually exist in offshore and onshore permafrost environments, marine sediments, and subglacial settings (Collett, 1993, 2002; Kvenvolden, 1993; Portnov et al., 2016; Ruppel and Kessler, 2017; Sloan Jr and Koh, 2008). These hydrates may contain the vast majority of methane in the world and account for nearly one-third of the globe's mobile organic carbon content (Beaudoin et al., 2014). The estimation of the entire volume of gas hydrates resources is nearly 3000 trillion cubic meters (TCM) (Boswell and Collett, 2011; Milkov, 2004). As a result, gas hydrates have attracted the concentration of numerous countries and regions as a new type of high potential energy (Chong et al., 2016; Merey, 2016).

Over the past decades, production tests of gas hydrates have been carried out in Messoyakha (Makogon et al., 2007), Mackenzie Delta (Kurihara et al., 2005, 2010; Majorowicz et al., 2012; Majorowicz and Osadetz, 2001), Alaska North Slope (Anderson et al., 2011; Collett et al., 2008; Hunter et al., 2011), Nankai Trough (Hamamoto et al., 2011; Jia et al., 2017; Miyakawa et al., 2014; Sun et al., 2016), and Shenhu area (Li et al., 2016, 2018; Wu and Wang, 2018). Through these investigations, it was found that gas hydrate accumulation is controlled by various factors, such as gas hydrate stability conditions, gas source, water, gas migration, reservoirs, and timing (Collett et al., 2009). Among these factors, gas migration pathways are critical links in

* Corresponding author. Hubei Key Laboratory of Marine Geological Resources, China University of Geosciences, Wuhan, 430074, China.
** Corresponding author. Gas Hydrate Engineering and Technology Center, Guangzhou Marine Geological Survey, Guangzhou, 510075, China
*E-mail addresses:* taojiang@cug.edu.cn (T. Jiang), yangczcug@163.com (C. Yang).

https://doi.org/10.1016/j.jngse.2020.103629
Received 20 July 2020; Received in revised form 25 August 2020; Accepted 22 September 2020
Available online 25 September 2020

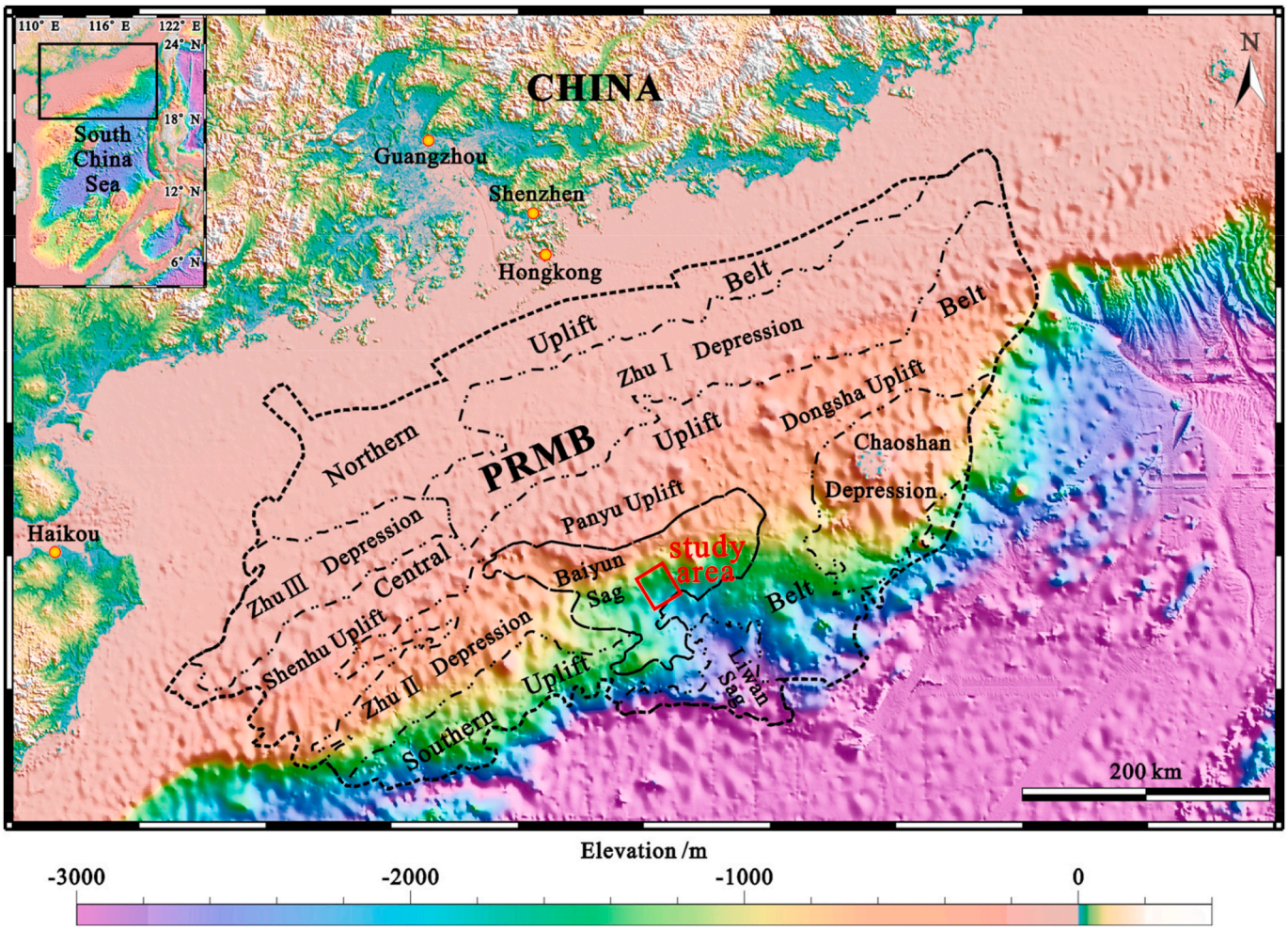


**Fig. 1.** Location of the study area (red rectangle) in the PRMB (black dashed lines), northern SCS (insert). PRMB: Pearl River Mouth Basin. SCS: South China Sea.

characterizing the fluid flow and gas hydrate accumulation and should be extensively studied. Methane required for gas hydrate accumulation can be originated from thermogenic and microbial origins and transported into the GHSZ (Collett et al., 2009; Milkov et al., 2005; Pohlman et al., 2009; Riedel et al., 2010). Many laboratory and field studies showed gas migration pathways were associated with fluid diapirs (Lei et al., 2011; Wang et al., 2004; Xie et al., 1999b), mud diapirs (Behrens, 1984; Hsu et al., 2017; Van Rensbergen et al., 1999; Wang and Huang, 2008), magma diapirs and igneous bodies (Cartwright et al., 2007; Schofield and Jolley, 2013; Sun et al., 2014), salt diapirs (Haines et al., 2017; Trusheim, 1960), fault systems (Inks et al., 2009) and gas chimneys (Chen et al., 2013; Choi et al., 2013; Hutchinson et al., 2009; Su et al., 2014, 2016, 2017; Sun et al., 2012, 2017; Wang et al., 2011). Among those analyses, gas chimneys as vertical gas migration pathways performed a critical role in gas hydrate accumulation in the marine environments.

The Baiyun Sag in the Pearl River Mouth Basin (PRMB) has become a principal hotspot for deep-water oil and gas exploration in the northern South China Sea (SCS) in recent years. Furthermore, the Shenhu area, located in the Baiyun Sag, has become the frontier of the studies on marine gas hydrate in China (Pang et al., 2009; Tian et al., 2019; Wang et al., 2014a). The GMGS has conducted several gas hydrate expeditions in the northern SCS in recent years, including 8 sites drilled in 2007 (GMGS1), 19 sites drilled in 2015 (GMGS3), and 11 sites drilled in 2016 (GMGS4) in the Shenhu area (Yang et al., 2017b, 2017c, 2017d). During these expeditions, GMGS has acquired a large number of cores, well logging data, and 2D and 3D seismic datasets. Also, gas hydrate production tests have been conducting in this regard from May to July in 2017, which have attracted the research interests of many scholars (Li et al., 2018; Liang et al., 2017; Wu and Wang, 2018). Many studies have also been carried out to determine the gas hydrate accumulation mechanism in the Shenhu area in recent years (Su et al., 2017; Wan et al., 2017; Zhang et al., 2018). Among them, the gas samples collected from hydrate-bearing zones during GMGS1 were interpreted to be of microbial origin. The carbon isotope of methane ($\delta^{13}C_1$) was between −60.9‰ and −56.7‰, and the hydrogen isotope of methane (δD) ranged from −199‰ to −191‰. This indicated that the methane was created from the microbial reduction of $CO_2$ (Zhu et al., 2013). Subsequently, samples of gas hydrate dissociation obtained from site W19 during GMGS3 suggested that gas was of mixed thermogenic and microbial origins. The $\delta^{13}C_1$ and δD values of pressure cores taken from site SC-01 in the Shenhu area during GMGS4 were between −50.9‰ and −46.46‰ and −177.69‰ to −148.9‰, respectively. This showed that methane from the gas hydrate was dominated by thermogenic origins (Wei et al., 2018; Zhang et al., 2017). Increasing pieces of evidence showed that thermogenic gas was a significant source of methane for gas hydrates in the Shenhu area.

On the basis of seismic data, Chen et al. (2013) identified gas chimneys, mud diapirs, and active faults as the three primary types of fluid flow systems in the Shenhu area. Among them, gas chimneys were significant fluid migration pathways for gas hydrate accumulation. Their genesis might have been related to the overpressured fluid release triggered by the Dongsha Event, which was largely influenced by the subduction and collision of the SCS towards the Philippine Sea plate (Xie

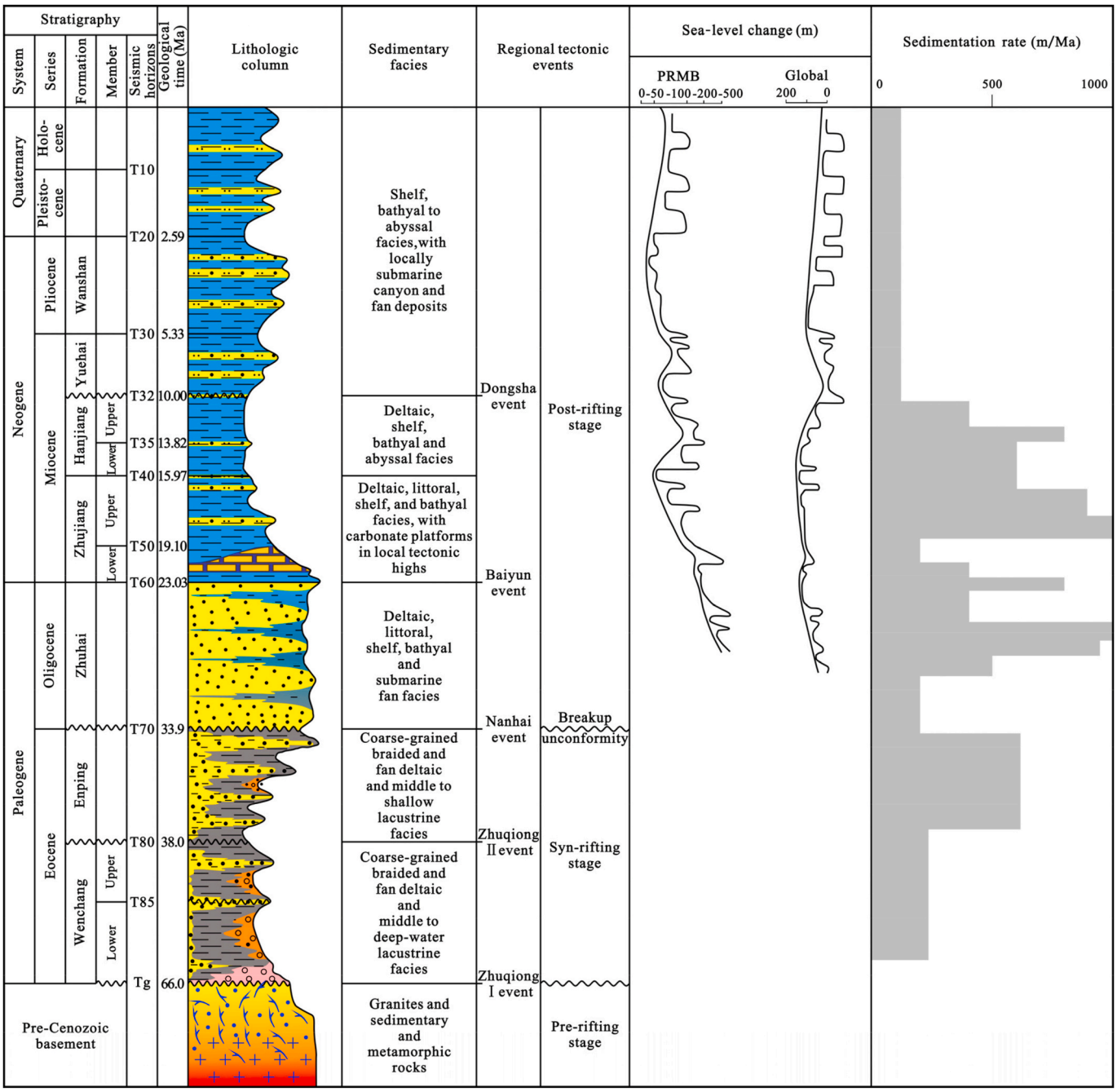


**Fig. 2.** Simplified chronological, stratigraphic, and tectonic columns in the PRMB (modified from Shi et al., 2014; Xie et al., 2013; Zhao et al., 2018). The sea-level curve was obtained from Pang et al. (2008) and Kong et al. (2018). Moreover, the ages of the sequence boundary were derived from He et al. (2017).

et al., 2017; Zhao et al., 2012). Through the analysis of the seismic data, Yang et al. (2015) and Su et al. (2016) reported that there were many small faults between the base of the gas hydrate stability zone (BGHSZ) and the head of gas chimneys, which could transport fluids upward into the GHSZ. Su et al. (2017) recognized vertical and lateral gas migration pathways. The vertical one included gas chimneys, mud diapirs, and large-scale faults, while the lateral one included detachment faults, normal faults, and permeable sediments. These studies suggested that gas from deeper sediments might have been transported upward by vertical pathways, then migrated laterally through normal faults. However, the detachment faults were most likely to act as gas escape pathways. Gas chimneys, normal faults, and polygonal faults were observed based on 3D seismic data. The release of overpressured fluids might have formed gas chimneys (Yang et al., 2017a). By comparing the fluid migration pathways between the GMGS1 and GMGS3 drilling areas, Zhang et al. (2018) reported that large-scale faults and mud diapirs might have transported the thermogenic gas upward into the GHSZ. These studies have shown that vertical gas migration pathways have performed a vital role in gas hydrate accumulation in the Shenhu area. They are also essential conduits for deep thermogenic and shallow microbial gas to transport into the GHSZ. However, the types of vertical gas migration pathways, genetic mechanisms, and specific effects on gas hydrate accumulation are required to be further studied.

In our work, high-resolution 3D seismic data newly obtained in 2018 and well logging data from GMGS1 and GMGS3 were utilized to characterize the gas chimneys and their implications on gas hydrate accumulation in the Shenhu area. The characterization of various types of gas chimneys was summarized, and their genetic mechanisms to

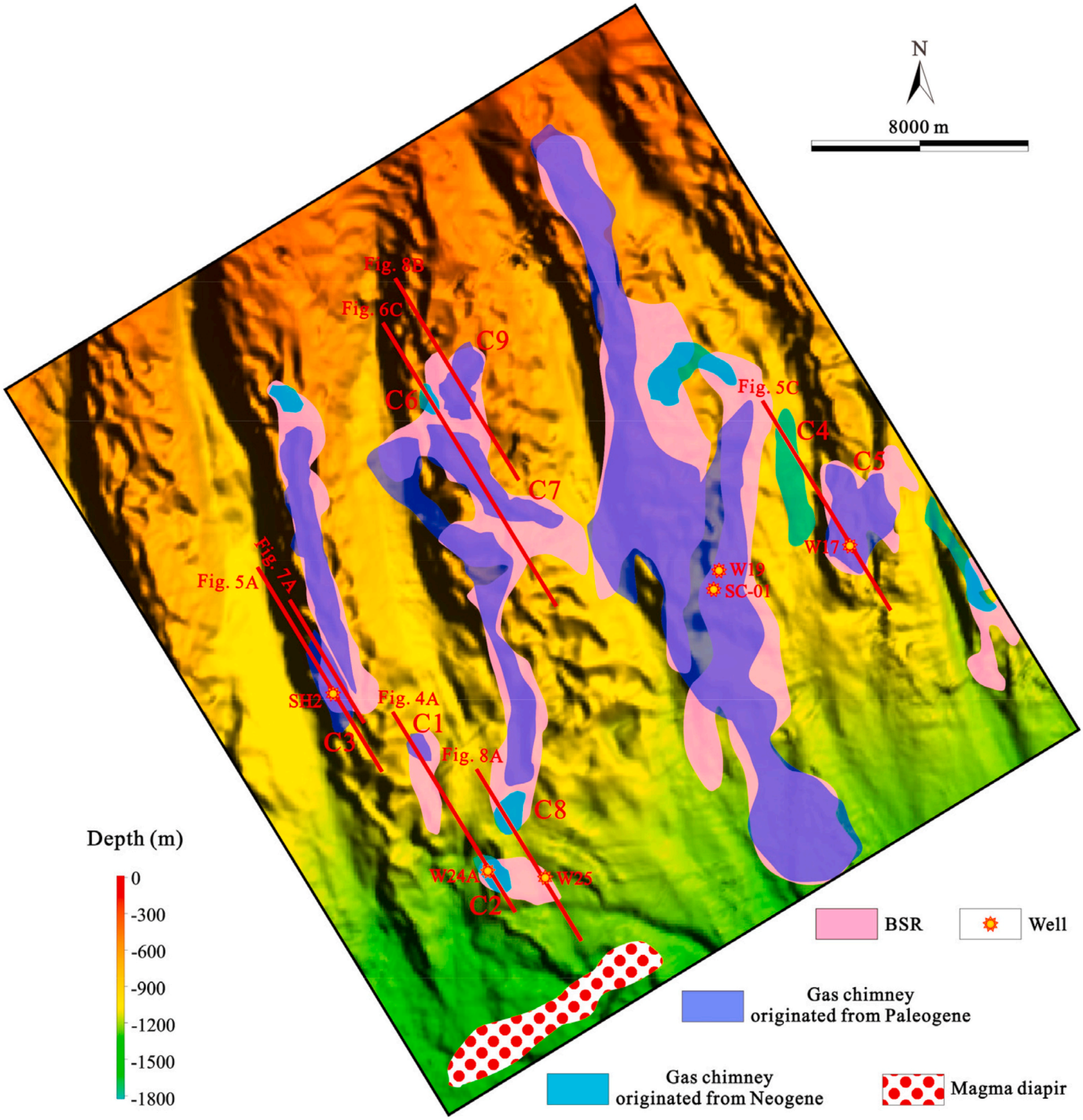


**Fig. 3.** Multi-beam map of the seafloor and the locations of gas hydrate drilling sites in the study area (modified from Jin et al., 2020; Wei et al., 2018; Yang et al., 2017b; Yang et al., 2017c; Yang et al., 2017d; Zhang et al., 2018; Zhang et al., 2020; Zhang et al., 2017). The distribution of BSR, gas chimneys, and diapiric structures were illustrated in the map. The map also shows the locations of gas chimneys C1 to C9. BSR: Bottom-Simulating Reflector.

subsequently determine the influence of different types of gas chimneys on gas hydrate accumulation were investigated. Finally, a geological model of gas hydrate accumulation was proposed.

## 2. Geological setting

The PRMB is the largest Cenozoic petroliferous basin in the northern SCS (Fig. 1), covering an area of about $19.38 \times 10^4$ km$^2$, which is located in the continental shelf to slope areas (He et al., 2017). The basin has undergone several tectonic events since the Cenozoic and has developed a series of fault systems and diapiric structures (Sun et al., 2008; Wang et al., 2006). Moreover, the basin has experienced 3 stages of the geological evolution: pre-rifting stage (pre-Cenozoic), syn-rifting stage (Eocene), and post-rifting stage (Oligocene to present) (Fig. 2) (He et al., 2017; Li et al., 2014). The Wenchang formation and Enping formation, the primary hydrocarbon sources in the PRMB, are mostly coarse-grained braided deltaic and lacustrine facies developed through the syn-rifting stage. The post-rifting stage consists of the Zhuhai, Zhujiang, Hanjiang, Yuehai, Wanshan formations, and Quaternary strata from bottom to top. Among them, the Hanjiang formation and Yuehai

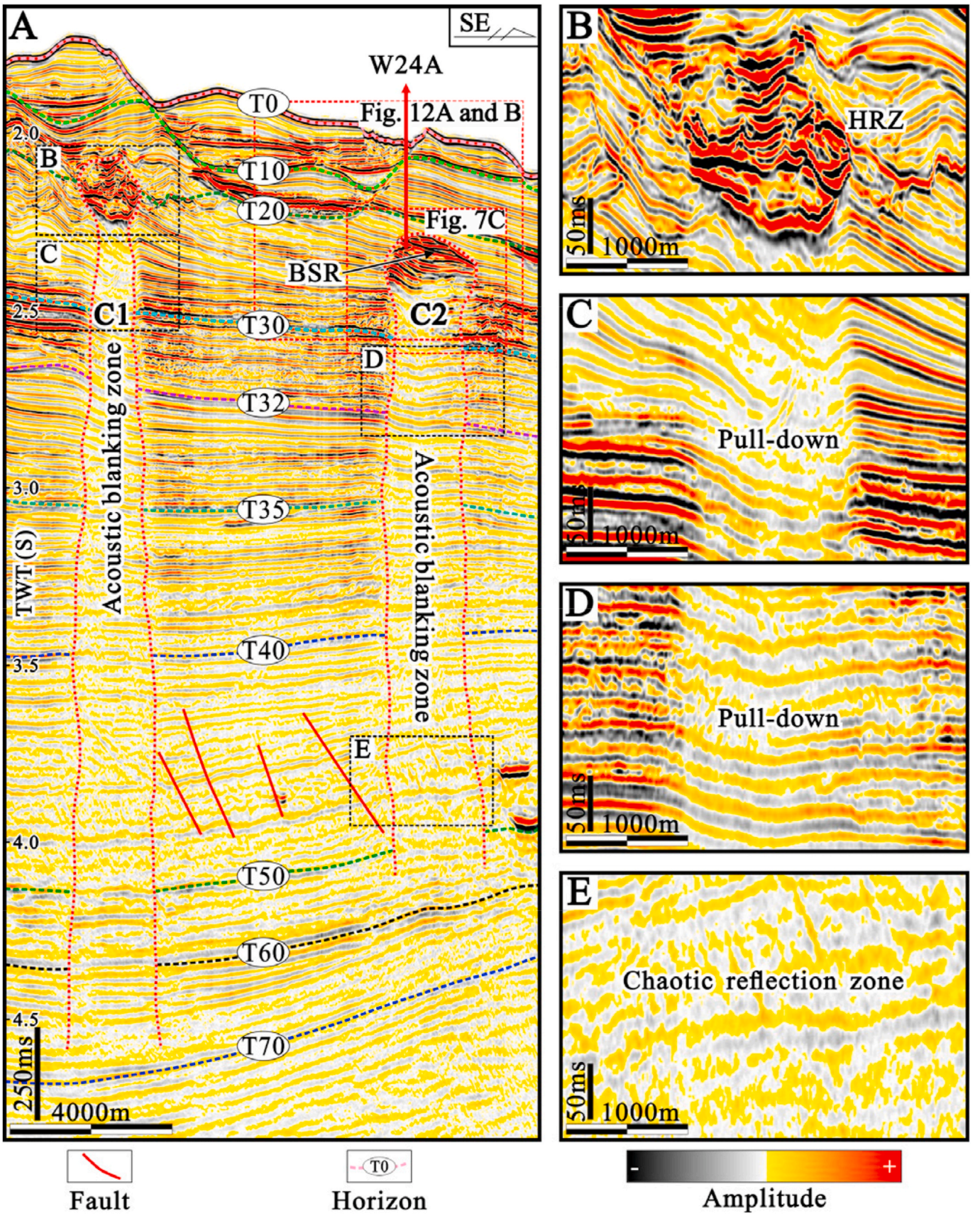


**Fig. 4.** Characteristics of gas chimneys C1 and C2. (A) Gas chimneys C1 and C2 on the seismic profile. (B and C) Internal reflection characteristics of gas chimney C1. (D and E) Internal reflection characteristics of gas chimney C2. See Fig. 3 for the location of Fig. 4A. The black dashed rectangles show the positions of Fig. 4B, C, D and E. The red dashed rectangles show the positions of Figs. 7C and 12A and B. HRZ: High-amplitude reflection zone.

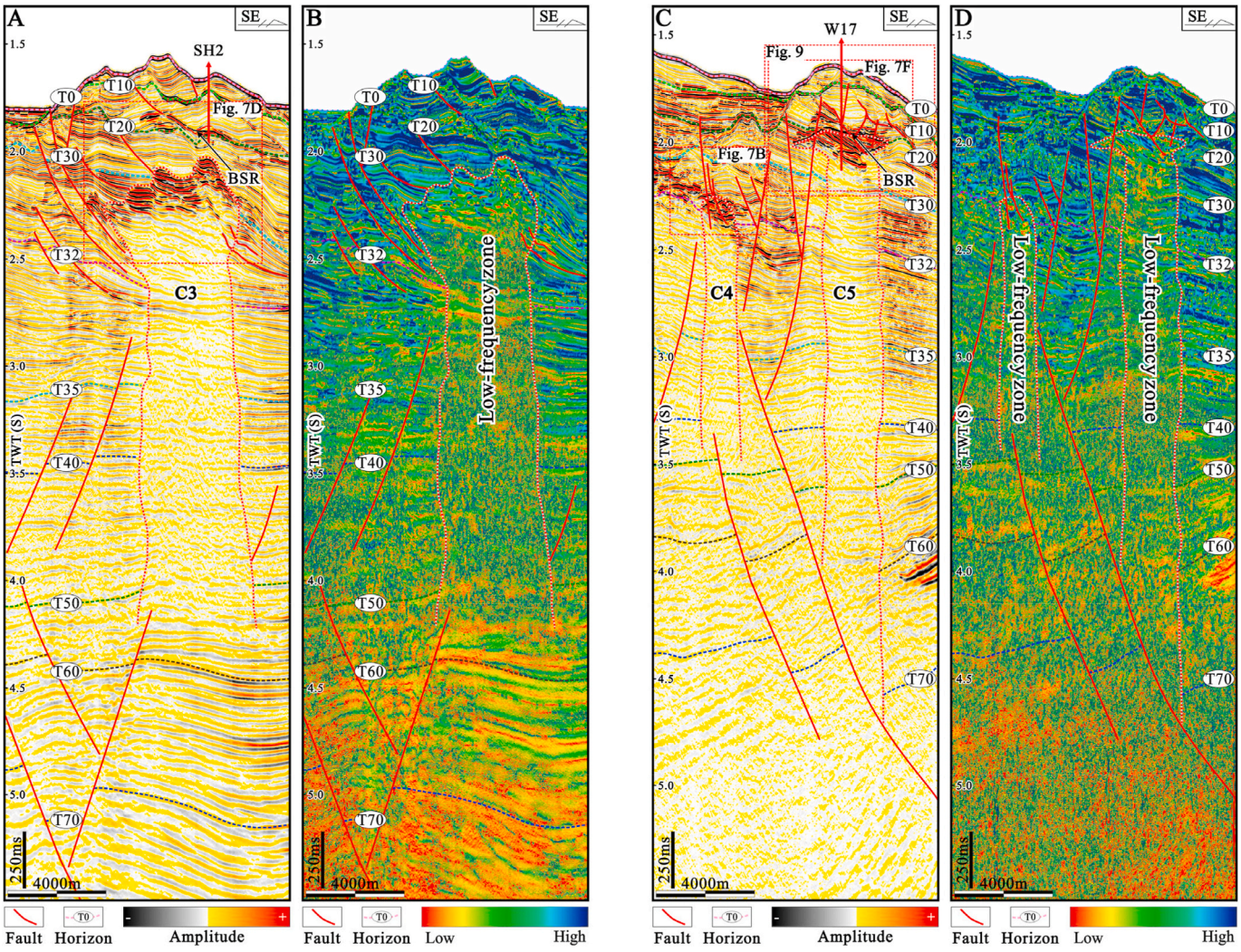


**Fig. 5.** Characteristics of gas chimneys C3, C4 and C5. (A and C) Gas chimneys C3, C4 and C5 on the seismic profiles, respectively. (B and D) Gas chimneys C3, C4 and C5 on the instantaneous frequency attribute profiles, respectively. The red dashed rectangles show the positions of Fig. 7B, D, F and 9. The low-frequency zone represents the gas chimney. See Fig. 3 for the locations of Fig. 5A and C.

formation are shelf, bathyal, and abyssal facies, which can be sources of microbial gas (He et al., 2017).

This study area was in the Shenhu area and geologically belonged to the Baiyun Sag, PRMB. Several submarine canyons existed in this area with an observable change in the seafloor topography (Figs. 1 and 3). The water depth ranged from 500 to 1700 m in this region, and the bottom temperature of the seabed was between 3.3 and 3.7 °C (Zhang et al., 2017). Based on the data acquired during GMGS1, the heat flow and geothermal gradient values were roughly from 62 to 98 mW/m$^2$ and 44–68 °C/km, respectively. The GHSZ drilled intervals were between 80 and 224 m indicating the geological conditions in this area were favorable for gas hydrate accumulation (Liang et al., 2014).

## 3. Data and method

In this research, the newly acquired high-resolution 3D seismic data in 2018 reached an area of ~800 km$^2$ (Fig. 3), while the primary frequency was about 60 Hz. These high-resolution 3D seismic data were obtained with a bin size of 12.5 m (inline direction) × 6.25 m (crossline direction) and a sampling interval of 2 ms. The 3D seismic data were processed for trace editing, bandpass filtering, amplitude preservation, and pre-stacking depth migration (Zhang et al., 2020). Then, Geoframe® was employed to interpret seismic data and extract seismic attributes, including instantaneous frequency and coherence slices. Whereas instantaneous frequency attributes can be used to identify fluids, coherence slices are commonly applied to study the spatial distribution characteristics of lithological anomalies and geological structures.

Numerous wells had been drilled by the GMGS in the Shenhu area, providing the basic borehole dataset to study gas hydrates. In this study, natural gamma-ray (GR) logging and resistivity (RES) logging data, acquired by the logging while drilling (LWD) operation during GMGS1 and GMGS3, were used for four sites to characterize the gas chimneys and their implications on gas hydrates.

10 horizons were traced based on the well-to-seismic ties to build the sequence stratigraphic framework in this study (He et al., 2017; Huang et al., 2018; Shi et al., 2014). Gas chimneys with various top shapes were then identified and characterized on the seismic profiles (i.e., instantaneous frequency attribute profiles) (Coren et al., 2001). Moreover, coherence slices of several horizons were also applied to analyze the gas chimneys (Yang et al., 2017a), and their genesis mechanism was determined. Finally, the impacts of the various types of gas chimneys on gas hydrates accumulation were analyzed, and an accumulation model for gas hydrates was proposed.

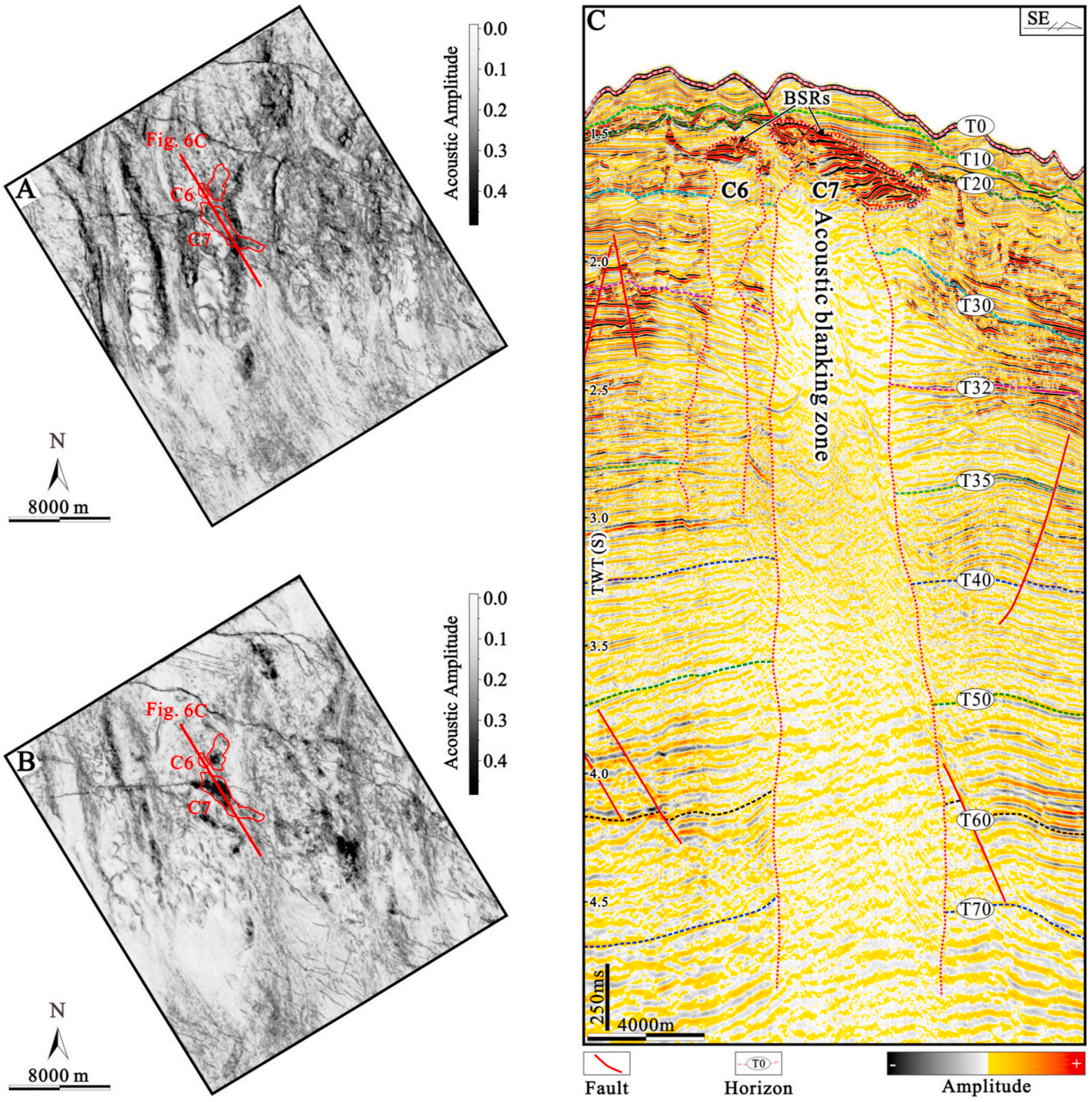


**Fig. 6.** Characteristics of gas chimneys C6 and C7. (A and B) Coherence slices of horizon T30 and T32, respectively. (C) Gas chimneys C6 and C7 on the seismic profile, respectively. See Fig. 3 for the location of Fig. 6C. BSRs: Bottom-Simulating Reflectors.

## 4. Results

### 4.1. Geophysical recognition of gas chimneys based on seismic data

#### 4.1.1. Seismic interpretation

On the basis of 2D and lower resolution 3D seismic data, gas migration pathways in the Shenhu area have been characterized previously (Chen et al., 2013; Su et al., 2014, 2016, 2017; Yang et al., 2015, 2017a). Numerous vertical blanking zones were recognized on the seismic profiles, which were considered as gas chimneys (Petersen et al., 2010; Zühlsdorff and Spieβ, 2004). In the study area, high-resolution 3D seismic data were employed to characterize gas chimneys. Gas chimneys C1 and C2 were readily identified from the seismic profile (Fig. 4). C1 and C2 are long columnar-shaped with acoustic blanking zones and high-amplitude reflection zones (HRZ) (Fig. 4A and B). The HRZ at the top of the gas chimney might have been formed by free gas accumulation (Chen et al., 2013; Qian et al., 2018; Wang et al., 2014a; Yang et al., 2015). Also, there were Bottom-Simulating Reflectors (BSRs) above the HRZ, which was a high-amplitude reflection interface caused by the difference in velocity when seismic waves propagate through the hydrate-bearing layer and the low-speed gas-bearing or water-bearing layer existing below it (Boswell et al., 2016; Portnov et al., 2020). In this research, the BSRs showed good correspondences with gas chimney. In the upper part of gas chimneys C1 and C2, “pull-down” seismic

**Table 1**
Primary parameters of gas chimneys C1 to C9. See Fig. 3 for the locations of gas chimneys. HRZ: High-amplitude reflection zone.

| Gas chimney | Seismic reflection characteristics | | | Top shapes | Origin strata | Top terminal strata |
|---|---|---|---|---|---|---|
| | Internal reflection (from bottom to top) | Continuity | Other anomalies | | | |
| C1 | Chaotic reflection zone, acoustic blanking zone, and HRZ | Rather continuous | Slight "pull-down" | Capsule-shaped | Zhuhai formation | Quaternary strata |
| C2 | | Rather continuous | "pull-down" | Dome-shaped | Zhujiang formation | Wanshan formation |
| C3 | Large chaotic reflection zone, acoustic blanking zone, and HRZ | Poorly continuous | / | Corolla-shaped | Wenchang-Enping formations | Wanshan formation |
| C4 | Large acoustic blanking zone, and HRZ | Poorly continuous | / | Dome-shaped | Zhujiang formation | Yuehai formation |
| C5 | Chaotic reflection zone, acoustic blanking zone and HRZ | Rather continuous | Slight "pull-down" | Mushroom-shaped | Wenchang-Enping formations | Quaternary strata |
| C6 | Chaotic reflection zone and HRZ | Rather continuous | / | Dome-shaped | Hanjiang formation | Wanshan formation |
| C7 | Chaotic reflection zone, large acoustic blanking zone, and HRZ | Poorly continuous | "pull-down" | Mushroom-shaped | Wenchang-Enping formations | Quaternary strata |
| C8 | Acoustic blanking zone, and HRZ | Rather continuous | "pull-down" | Dome-shaped | Hanjiang formation | Quaternary strata |
| C9 | Chaotic reflection zone, large acoustic blanking zone, and HRZ | Poorly continuous | "pull-down" | Capsule-shaped | Wenchang-Enping formations | Quaternary strata |

anomalies were clearly observed (Fig. 4C and D). Moreover, a chaotic reflection zone was identified at the bottom of C2 (Fig. 4E). These low-amplitude reflectors were useful for identifying gas chimneys.

#### 4.1.2. *Instantaneous frequency attribute analysis*

The instantaneous frequency attributes show an abnormal lower frequency zone on the seismic profile if there are focused fluids such as

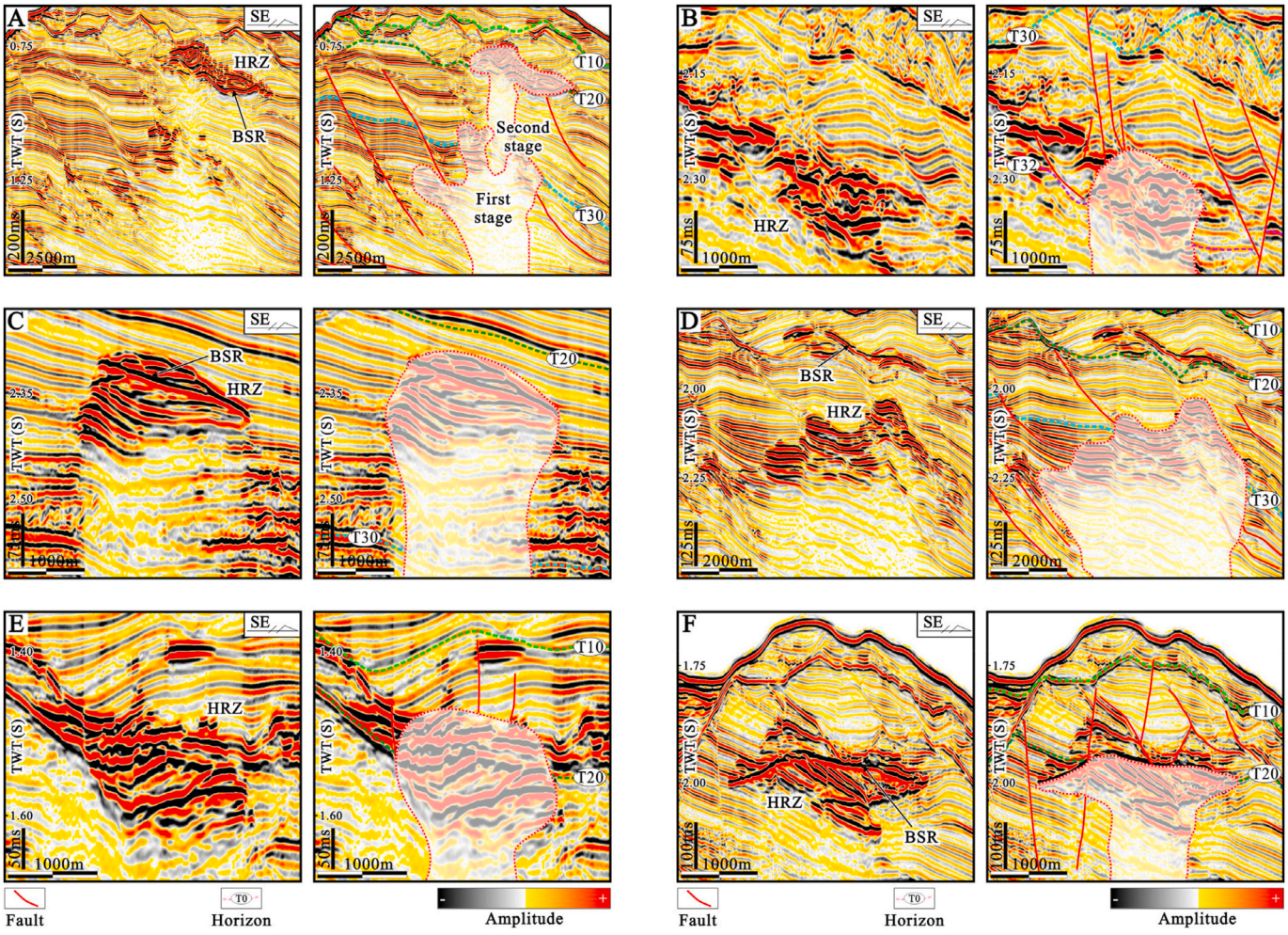


**Fig. 7.** Gas chimneys with various top shapes and terminal strata. (A) Two stages of activities of gas chimney C3. (B) Gas chimney C4 terminated in the Yuehai formation. (C) Dome-shaped gas chimney. (D) Corolla-shaped gas chimney. (E) Capsule-shaped gas chimney. (F) Mushroom-shaped gas chimney. Detailed characteristics of different gas chimneys are presented in Table 1. See Figs. 3–5 and 8 for the locations of Fig. 7A–F, respectively.

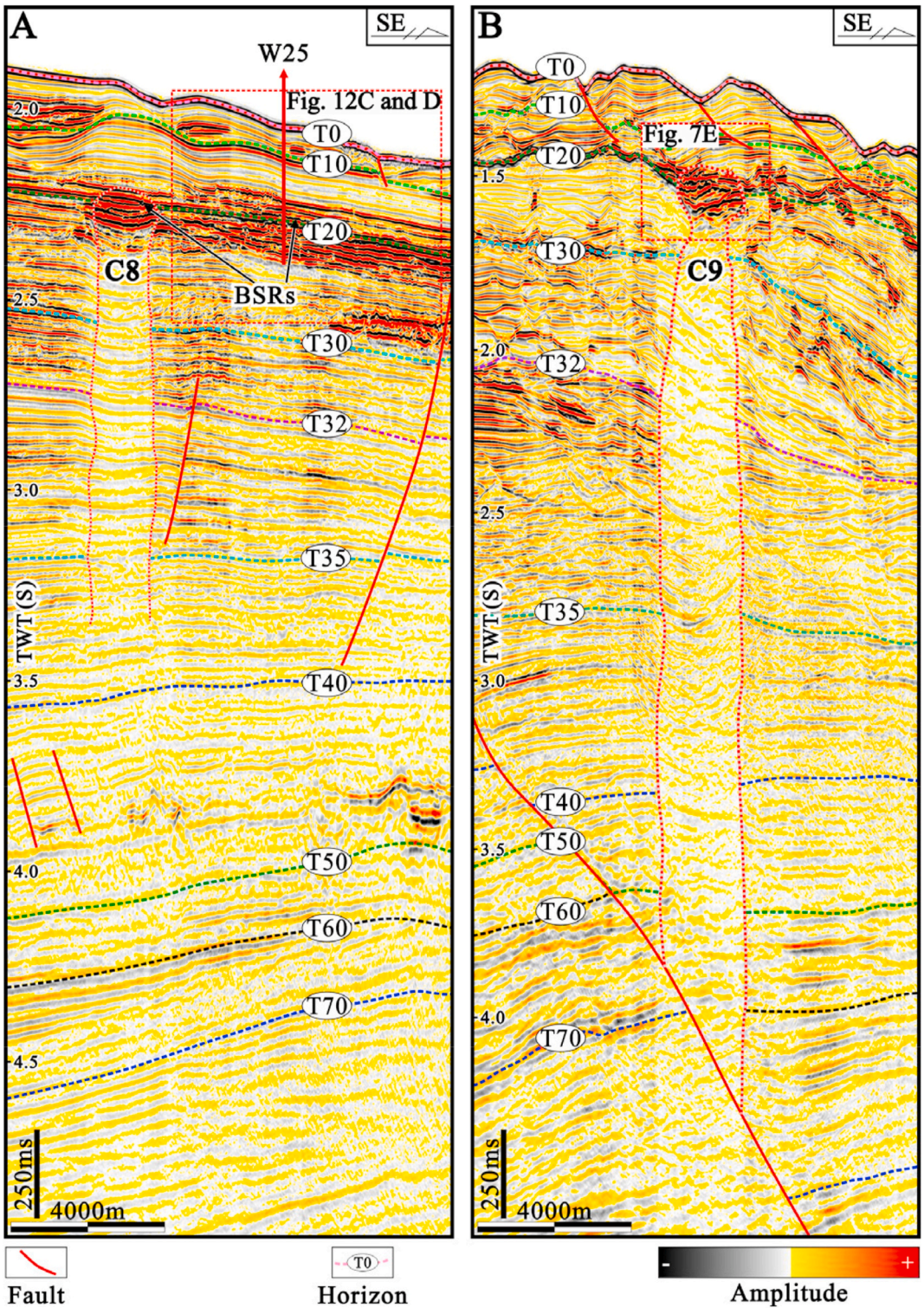


**Fig. 8.** Characteristics of gas chimneys C8 and C9. (A and B) Gas chimneys C8 and C9 on the seismic profiles, respectively. The red dashed rectangles show the positions of Figs. 7E and 12C and D. See the location of Fig. 8A and B in Fig. 3.

free gas in the sediments, which were used for the identification of gas chimneys C3 and C5 (Fig. 5). In general, when the sediments contain free gas and oil, they have a strong attenuation impact on the high-frequency seismic energy. This will lead to a decrease in the instantaneous frequency (Coren et al., 2001; Yang et al., 2015). Gas chimneys in the study area indicated by the low-frequency zones would present the instantaneous frequency attribute profiles (Fig. 5B and D). It can be seen from Fig. 5B and D that the low-frequency zones have a clear consistency with respect to the locations of the gas chimneys (Fig. 5A and C). This provided another way to identify the gas chimneys in the study area.

#### 4.1.3. *Coherence slices of horizons analysis*

A coherence slice is a seismic attribute that describes the lateral heterogeneity of the strata and lithology by using the variation in the coherence values of the seismic signals. Free gas inside the body of gas chimneys causes the seismic signals and sediment properties to be quite

different from the surrounding sediments and forms the acoustic blanking zones (Fig. 6). This lays the foundation for identifying the gas chimneys by coherence slices (Bahorich et al., 1995; Chopra, 2002). The acoustic blanking zone inside the body of gas chimney C7 in Fig. 6C could cause an abnormal higher acoustic amplitude zone, enabling it to be clearly identified on the coherence slices of horizons T30 and T32 (Fig. 6A and B).

### 4.2. Characteristics of gas chimneys

In the study area, gas chimneys were widely distributed on the ridges of submarine canyons, mostly NNW-trending, and appeared to be correlated with the distribution of the BSRs (Fig. 3). To analyze the gas chimneys and their implication on the accumulation of gas hydrates, the top shapes, original strata, top terminal strata of gas chimneys, and seismic reflection characteristics were applied to characterize the gas chimneys C1 to C9 (Table 1) (Hsu et al., 2017; Rapoport et al., 1986; Yang et al., 2015, 2017a).

#### 4.2.1. Top shapes of gas chimneys

Based on their internal reflection characteristics and top shapes, four types of gas chimneys with various top shapes were identified in the study area, including dome-shaped, corolla-shaped, capsule-shaped, and mushroom-shaped (Fig. 7). Gas chimney C2 was dome-shaped, with a chaotic reflection zone, an acoustic blanking zone, "pull-down" seismic events, and an HRZ (Figs. 4A and 7C). Also, the dome-shaped top was likely to be formed by free gas accumulation. The internal reflection was chaotic in the corolla-shaped gas chimney C3, and enhanced reflectors could be seen at the top (Figs. 5A and 7D). They are possibly caused by the lateral migration of free gas. They were also the most apparent feature of the corolla-shaped gas chimneys. The internal reflection characteristics of the capsule-shaped gas chimney C9 and dome-shaped gas chimney C2 were similar, both of them were long columnar and contained an HRZ at the top (Figs. 7E and 8B).

Mushroom-shaped gas chimneys had widely developed in this area and were the most numerous type of gas chimneys. Gas chimney C5 was a typical mushroom-shaped gas chimney, which was long column-shaped (Figs. 5C and 7F). The internal seismic reflection was characterized by a chaotic reflection zone, an acoustic blanking zone, and a mushroom-shaped HRZ from bottom to top. A slight "pull-down" anomaly could also be seen. The seismic events inside gas chimney C5 were rather continuous, and the enhanced reflectors at the top were caused by the decrease in acoustic velocity because of gas hydrates and free gas (Li et al., 2018; Qian et al., 2018) (Fig. 7F).

#### 4.2.2. Timing of gas chimneys

The original strata at the root and the terminal strata at the top of the gas chimneys should be considered. Through these studies, it could be determined where gas sources and sinks are located. On seismic profiles, the internal reflection characteristics of gas chimneys were generally chaotic reflection zones. Combined with instantaneous frequency attributes and coherence slices of several horizons, gas chimneys in the study area were divided into two categories on the basis of their original strata: gas chimneys originated from the Paleogene and gas chimneys originated from the Neogene (Figs. 3 and 8). Among them, most of the gas chimneys were originated from the Paleogene Wenchang and Enping formations, in which substantial sets of lacustrine mudstones were deposited, rich in organic matters and gas. The gas chimneys originated in the Neogene were within the Zhujiang formation and Hanjiang formation, which have developed marine mudstones. Gas chimney C8 was dome-shaped and originated from the Hanjiang formation, indicating that the gas had accumulated at the top was principally from a microbial origin (Fig. 8A). At the same time, C9 was of thermogenic origin (Fig. 8B) (Zhu et al., 2013).

The top of gas chimneys in the study area all terminated in the strata above the Middle Miocene, including the Yuehai formation, Wanshan

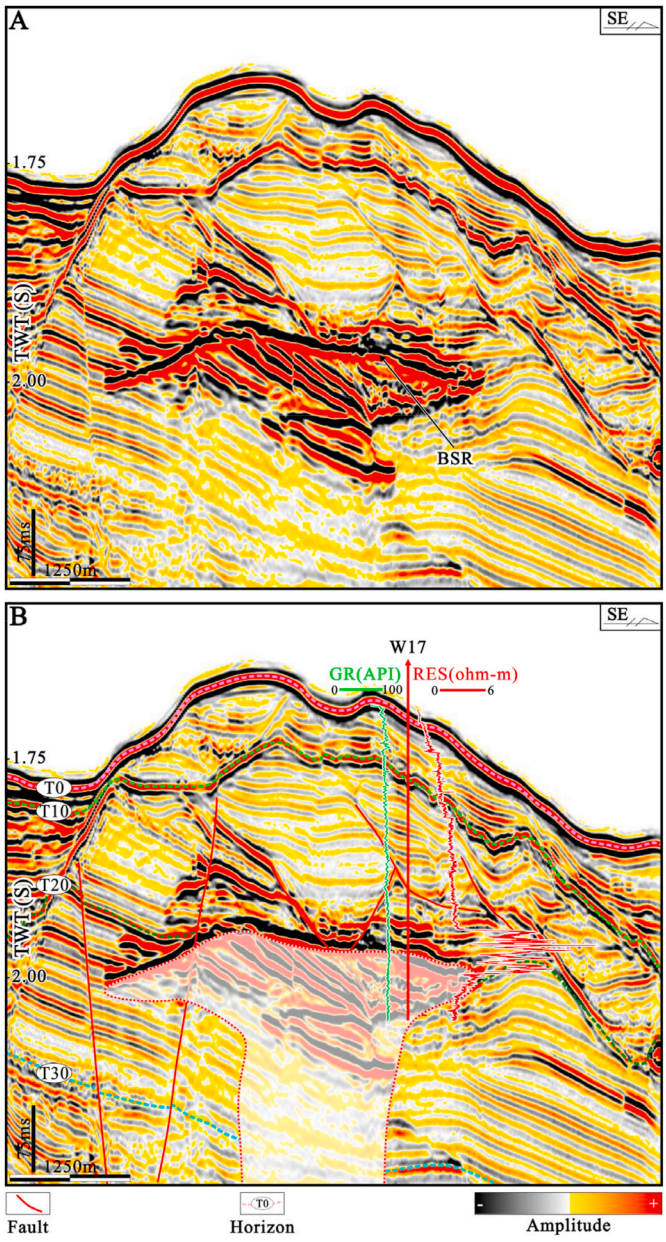


**Fig. 9.** Synthetic well-to-seismic ties of Site W17 (modified from Liang et al., 2017; Zhang et al., 2020). The BSR at the top of C5 can be seen in Fig. 9A. See the location of Fig. 9 in Fig. 5C. GR: Gamma-ray. RES: Resistivity.

formation, and Quaternary strata (Table 1). Most gas chimneys, such as C1, C5, C7, C8, and C9, had pierced into horizon T20 and terminated in the Quaternary strata. Based on drilling results, it was determined that the gas hydrate reservoirs were primarily within the Quaternary strata with fine-grained sediments, and suitable temperature and pressure in the Shenhu area (Li et al., 2019; Liang et al., 2017; Liu et al., 2017; Wang et al., 2014b). Through the seismic profiles, the top terminal strata of gas chimneys could be more clearly distinguished (Fig. 7), and as noted in Fig. 7A, gas chimney C3 showed signs of reactivation. The top of C3 was in the Wanshan formation during the Pliocene at the first stage, and the second stage developed in the Quaternary, indicating the timing of fluid activities in this area.

In this work, through studying the origin and top terminal strata of gas chimneys C1 to C9, it was revealed that the deeper the origin of the gas chimneys, the shallower the top terminal strata; and the shallower the root, the deeper the top strata. For example, gas chimney C5 was

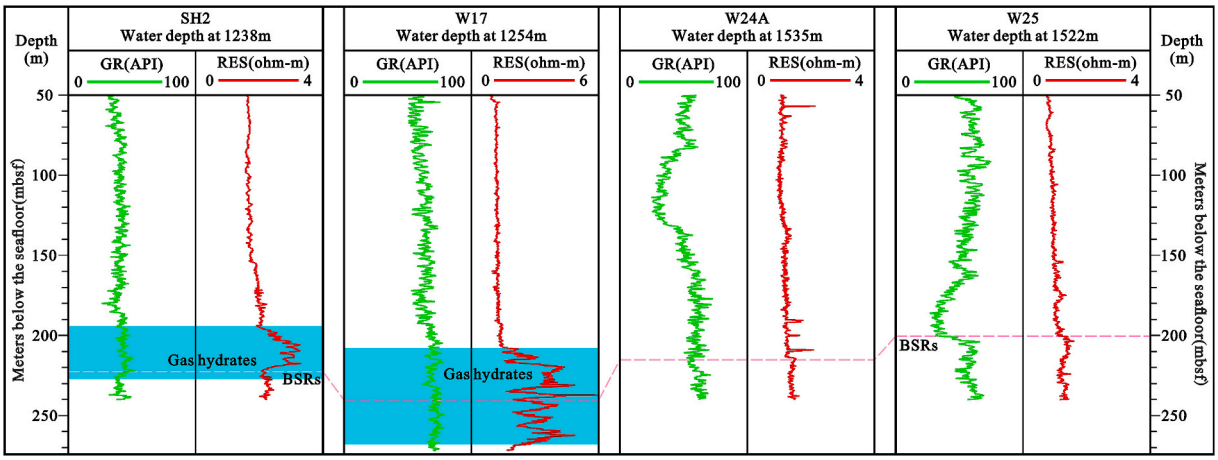


**Fig. 10.** Summary of well log curves from sites SH2 to W25, respectively. The GR and RES curves of SH2 and W17 were modified from Wang et al. (2014a), Su et al. (2016), Liang et al. (2017), and Yang et al. (2017d). The pink dashed line shows the BSRs identified from seismic data, and the cyan rectangles show the gas hydrates identified from seismic and logging data. See Fig. 3 for the locations of SH2 to W25, respectively.

originated from the Wenchang and Enping formations and terminated in the Quaternary strata, and C4 was originated from the Zhujiang formation and terminated in the Yuehai formation.

### 4.3. Characteristics and distribution of gas hydrates

#### 4.3.1. Seismic characteristics of gas hydrates

In this research, we used BSRs to infer gas hydrates from seismic profiles. The appearances of BSRs usually indicate that a large quantity of free gas has accumulated under the hydrate-bearing layer, and they are generally considered to be the BGHSZ (Boswell et al., 2016; Portnov et al., 2020). The spatial distribution of the BSR follows seafloor topography, but the reflection polarity is just the opposite. Furthermore, in regions with oblique layering, it can intersect sedimentary strata. In the study area, the BSRs exhibited a wide range of distributions, mostly along the ridges of canyons. They showed a high degree of coincidence with gas chimneys' distribution. The coincidence was due in no small amount of free gas at the top of gas chimneys, indicating that the gas hydrates had a sufficient gas source (Figs. 4–6 and 9).

On the seismic profile, it could be clearly observed that the BSR had high-amplitude reflections opposite to the polarity of the seafloor. Given these data, there was a high probability that gas hydrates formed above the BSR (Fig. 9A). Wells were drilled and cores were collected above the gas chimney C5, and both the LWD data and cores confirmed the existence of gas hydrates (Liang et al., 2017). As shown in Fig. 9B, site W17 had been drilled at gas chimney C5 and the gamma-ray (GR) logs changed slightly, which suggested that the lithology changed a little. However, the abnormal resistivity increase in logs was obviously affected by the hydrate layer.

#### 4.3.2. Log characteristics of gas hydrates

Gas hydrates are solid compounds and not easily-conductive, and display high P-wave velocity and high resistivity anomalies in the logging data (Fang et al., 2017; Peng et al., 2018). Therefore, acoustic and resistivity logging are the most effective methods to identify gas hydrate. In this study, four wells with GR and RES logging data were employed as the basis for recognizing gas hydrates (Fig. 10). Sites W17, W24A, and W25 were drilled during GMGS3 while site SH2 was drilled during GMGS1 (Jin et al., 2020; Yang et al., 2017b, 2017c, 2017d; Zhang et al., 2020). Among them, the water depth of SH2 and W17 was approximately 1200 m, and the GR curve did not change substantially. However, the RES curve showed a considerable abnormal resistivity increase in about 200 m below the seafloor (mbsf). The resistivity in W17 increased from 1.4 to 6.3 Ω-m, showing the existence of thick hydrate layers. Site W24A drilled at the water depth of 1535 m, and the GR curve was bell-shaped from 80 to 130 mbsf, which indicated that the grain size of sediments was fining-upward. The RES curve had several peaks, indicating that thin gas hydrate layers (less than 5 m) might be present below 180 mbsf, but no thick hydrate layer was found. Moreover, site W25 had a water depth of 1522 m, and the GR curve also showed bell-shaped at around 200 mbsf, similar to W24A. The RES curve was basically unchanged, and no layered hydrates were formed. Furthermore, studies have shown that gas hydrates mostly occurred in fine-grained sediments in the Shenhu area, such as silty clay and clayey silt, and the sedimentary facies were dominated by natural levee (Li et al., 2019; Zhong et al., 2017).

## 5. Discussion

### 5.1. Evolution of gas chimneys in the shenhu area

The structural evolutions of gas migration pathways such as diapirs in the Yinggehai Basin, Baram delta, and other areas have been previously constructed (Lei et al., 2011; Van Rensbergen et al., 1999; Xie et al., 1999a, 1999b). In this research, five stages were given to illustrate the evolution of gas chimneys based on the characteristics of the gas chimneys and tectono-sedimentary evolution (Fig. 11).

#### 5.1.1. Stage 1- hydrocarbon accumulation (oligocene to Middle Miocene)

The Shenhu area lies in the Baiyun Sag (Fig. 3), which is the crucial area for deep-water hydrocarbon exploration in the PRMB, and many large gas fields have been discovered in that location (He et al., 2017). The total area of Baiyun Sag is approximately $2 \times 10^4$ km$^2$, with the sedimentary thickness is larger than 10 km (Zeng et al., 2019). The lacustrine strata of the Wenchang and Enping formations, with high hydrocarbon generation potential and rich organic matter, are the primary source rocks with a maximum thickness of 7 km (Fig. 11A) (Mi et al., 2018; Shi et al., 2014). The Wenchang formation, which was deposited in the Eocene, had a major hydrocarbon generation window from 33.9 to 16.0 Ma. Moreover, the Enping formation, which was the main contributor to gas in the PRMB, was from 23.0 to 10.0 Ma. Consequently, a large number of hydrocarbon fluids accumulated in the sag up to the Middle Miocene (Mi et al., 2018; Pang et al., 2018).

#### 5.1.2. Stage 2- overpressure formation (oligocene to Late Miocene)

The hydrocarbon generation by transforming kerogen to oil and gas and also the compaction disequilibrium are essential for overpressure generation in the sedimentary basins (Kong et al., 2018; Swarbrick et al.,

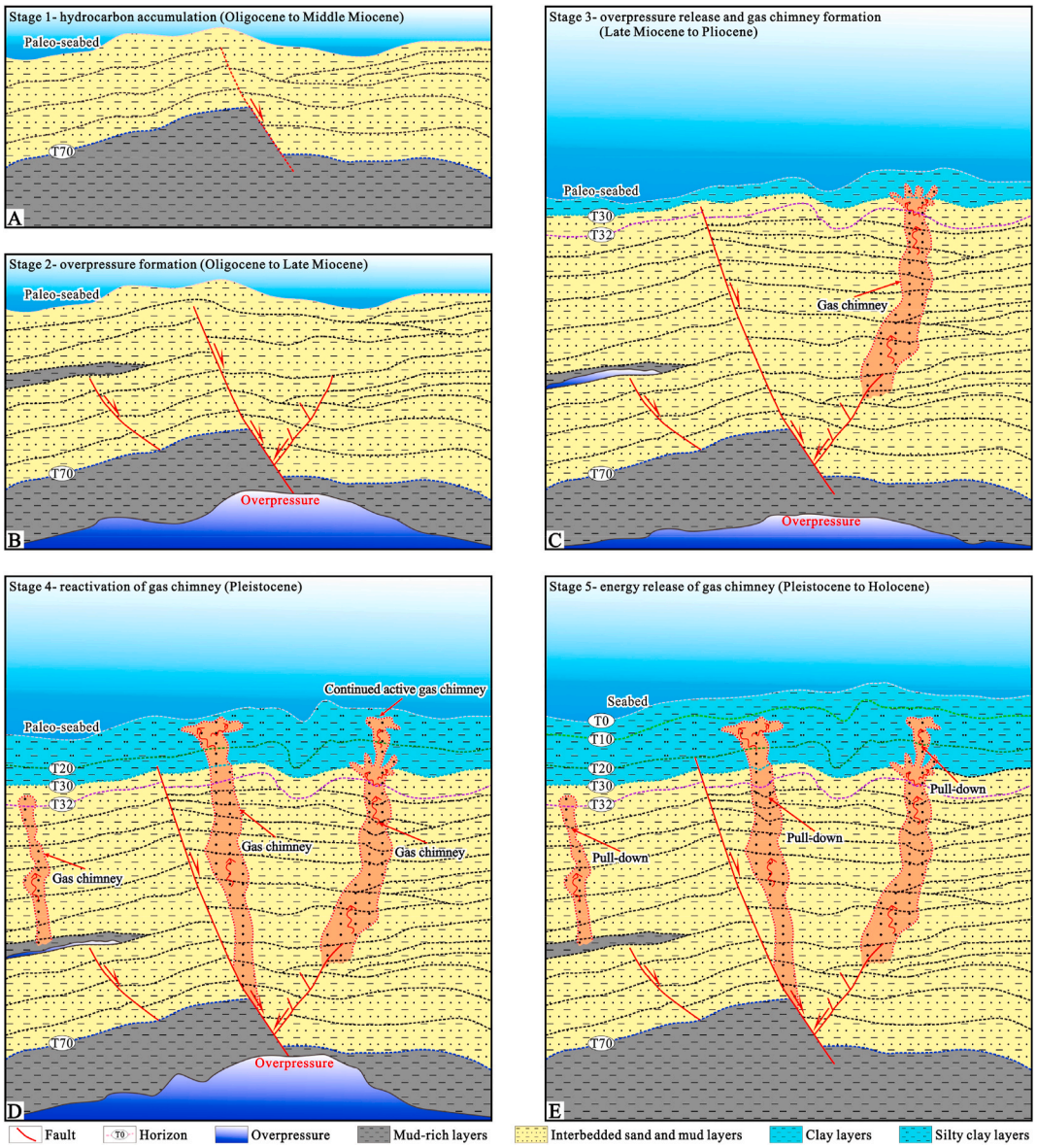


**Fig. 11.** Gas chimney's evolutionary model in the Shenhu area. (A) Stage 1, a large number of hydrocarbons accumulated in the lacustrine strata of the Wenchang formation and Enping formation from the Oligocene to Middle Miocene. (B) Stage 2, compaction disequilibrium caused by high sedimentation rates, and combined with the hydrocarbons accumulated during stage 1 in the Baiyun Sag will form overpressure. (C) Stage 3, the gas chimney formed when the release of overpressure triggered by the Dongsha event in the Late Miocene. (D) Stage 4, hydrocarbons accumulated in the deep formations via the release of overpressure caused the continued active gas chimney. (E) Stage 5, the energy of gas chimneys and overpressure gradually weakened and ceased to be active.

2001). Studies have shown that overpressure has formed in the Baiyun Sag, which has chiefly distributed within the Wenchang and Enping formations in the main sub-sag (Guo et al., 2016; Kong et al., 2018; Shi et al., 2007). Xie et al. (2013) identified three rapid and three slow deposition stages through the analysis of the sedimentary evolution in the central Baiyun Sag. The three rapid deposition stages were predominantly in Eocene, Oligocene, and Early-Middle Miocene. During the first rapid sedimentation stage, the Wenchang and Enping formations had deposited a significant thickness of lacustrine fine-grained mud sediments with the highest sedimentation rate of 600 m/Ma. Such a high sedimentation rate likely resulted in the compaction disequilibrium and increased the formation pressure (Audet and McConnell, 1992). Additionally, source rocks such as the Wenchang and Enping formations began to enter the hydrocarbon generation threshold, and the accumulation of hydrocarbon fluids began to increase the formation pressure. Under the combined action of compaction disequilibrium and hydrocarbon generation, overpressure had formed (Fig. 11B).

### *5.1.3. Stage 3- overpressure release and gas chimney formation (Late Miocene to pliocene)*

Episodic overpressured activities are believed to have developed in the study area, and the release of overpressure triggered by the Dongsha event in the Late Miocene has been recognized by many scholars (Guo et al., 2016; Kong et al., 2018; Mi et al., 2018; Ping et al., 2019; Shi et al., 2007). The release of overpressure is generally related to fluid migration (Judd and Hovland, 2009). When the overpressure was released due to the hydrocarbon expulsion of the source rocks, a large number of fluids within the strata migrated vertically through the weak zones and faults into shallow strata by piercing into the overlying strata. This caused the formation of a gas chimney (Lei et al., 2011; Van Rensbergen et al., 1999; Xie et al., 1999b). Since the Late Miocene, the release of overpressure was closer to the hydrocarbon charging stage (5.5–0 Ma). It coincided with the timing of the gas chimneys' activities in the study area, which further illustrated that the gas chimneys were associated with overpressured fluid activities (Fig. 11C) (Kong et al., 2018; Mi

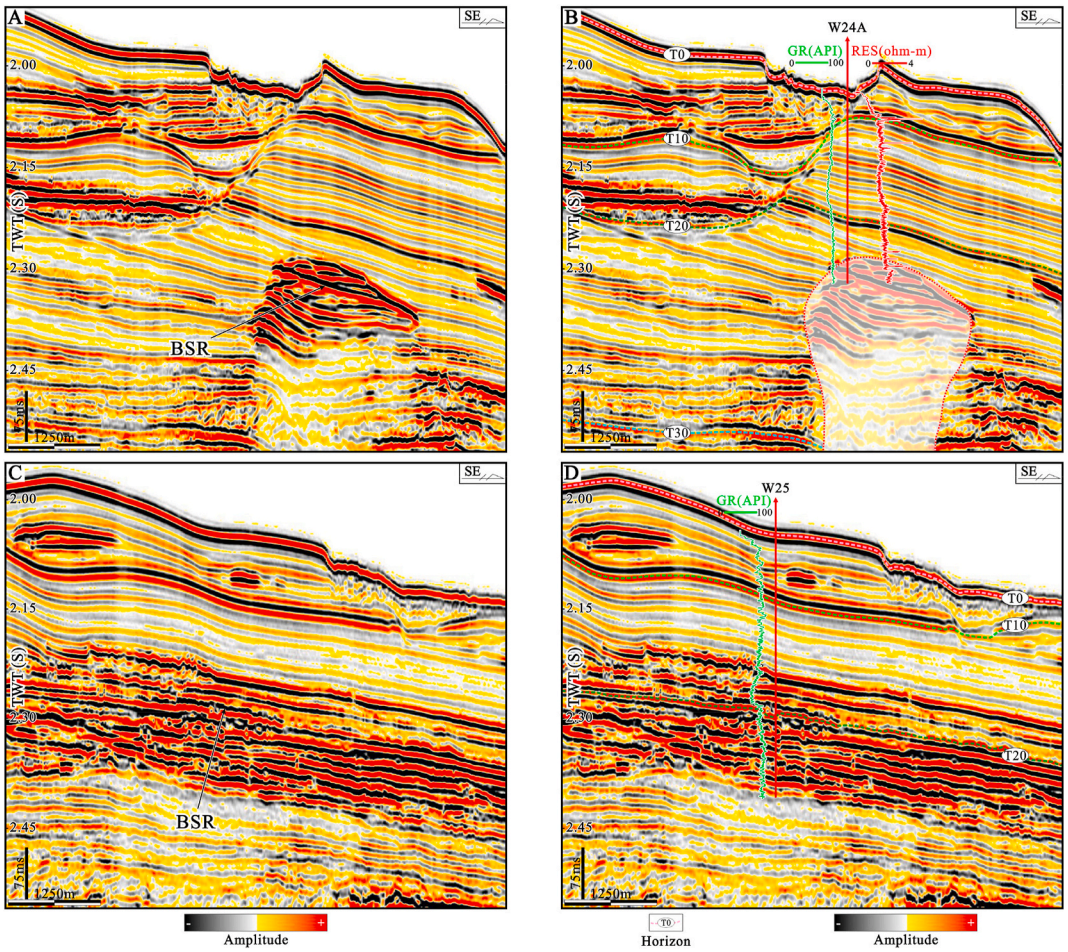


**Fig. 12.** Synthetic well-to-seismic ties of sites W24A and W25. (A and B) The results showed that there was no thick hydrate layer above gas chimney C2, but thin hydrate layers might be present. (C and D) No gas chimney formed, no apparent resistivity anomalies (Fig. 10), and no layered hydrate was found at W25. See Figs. 4 and 8 for the locations of Fig. 12A–D, respectively.

et al., 2018).

#### 5.1.4. Stage 4- reactivation of gas chimney (pleistocene)

Guo et al. (2016) proposed that there have been episodic overpressure releases since the Late Miocene, and the last one ranged from 2.0 to 0 Ma, which comparatively coincided with the second stage activity of gas chimney in the study area (Figs. 7A and 11D). Hydrocarbon fluids accumulating in the deep formations via the release of overpressure caused the reactivation of gas chimney, and transportation of a large amount of gas upward into the GHSZ, which performed a vital role in gas hydrates accumulation.

#### 5.1.5. Stage 5- energy release of gas chimney (pleistocene to holocene)

During this stage, the energy of gas chimneys and overpressure gradually weakened and ultimately ceased to be active. Inside the gas chimney, the pull-down seismic anomalies formed because of gas (Fig. 11D and E), and the gas accumulated at the top formed enhanced reflectors (Fig. 7), which ended the gas chimney's activity.

### 5.2. Impacts of gas chimneys on gas hydrates

The use of wells to analyze the characteristics of gas hydrates occurrence has been described previously (Fig. 10). Using W17, W24A, and W25, the influences of gas chimneys on gas hydrates are discussed below.

Site W17 was drilled at gas chimney C5 during GMGS3 (Fig. 5C), and a thick hydrate layer was confirmed to exist on and above the top of C5 (Figs. 9 and 10). Unlike the gas chimney C2, C5 was defined to be mushroom-shaped, originated from the Wenchang and Enping formations, and terminated in the Quaternary strata (Table 1). The Wenchang and Enping formations are source rocks, generating a large number of hydrocarbon gas (Mi et al., 2018; Pang et al., 2018). Moreover, Quaternary strata are the primary reservoirs for gas hydrates (Wei et al., 2018; Yang et al., 2017d). Gas chimney C5, which had directly connected the deep hydrocarbon source rocks and shallow gas hydrate reservoirs, was a pathway for gas migration. The sufficient gas and efficient transporting pathways were the keys to the presence of thick hydrate layer.

Site W24A was drilled at gas chimney C2 during GMGS3 (Fig. 4A), and thin hydrate layers may have been present as indicated by the logging data (Figs. 10 and 12A and B). Gas chimney C2, as a vertical migration pathway, transported gas upward into the GHSZ for gas hydrates accumulation. As summarized in Table 1, C2 was dome-shaped, originated from the Neogene Zhujiang formation, and terminated in the Neogene Wanshan formation. The Zhujiang formation developed sedimentary systems such as a shelf-margin delta and a channelized submarine fan, with coarse-grained sediments (Tian et al., 2019), which was the vast reservoir in the PRMB, but not the source rocks (Mi et al., 2018). Thus, the insufficiency of the hydrocarbon fluids made the gas chimney energy incapable of piercing into the Quaternary strata, and the shortage of the gas supply led to the occurrence of thin hydrate layers.

Site W25 was drilled into no chimney during GMGS3 (Fig. 8A), and no gas hydrate was found at this site (Fig. 10). While high-amplitude

**Table 2**
Characteristics of drilling sites, gas chimneys, and gas hydrate. See Fig. 3 for the locations of sites W17, W24A, and W25.

| Site | Gas chimney | Origin strata of gas chimney | Top terminal strata of gas chimney | Reflection characteristics of the target layer | BSR | Logging | Gas hydrate |
|---|---|---|---|---|---|---|---|
| W17 | C5 | Wenchang-Enping formations (Paleogene) | Quaternary strata (Quarternary) | Enhanced reflectors | Obvious and directly connected to the top of gas chimney | Resistivity anomalies | Thick hydrate layer |
| W24A | C2 | Zhujiang formation (Neogene) | Wanshan formation (Neogene) | Enhanced reflectors | Obvious and directly connected to the top of gas chimney | Slight resistivity anomalies | Thin hydrate layer |
| W25 | None | | | Enhanced reflectors | Obvious | Inconspicuous | None |

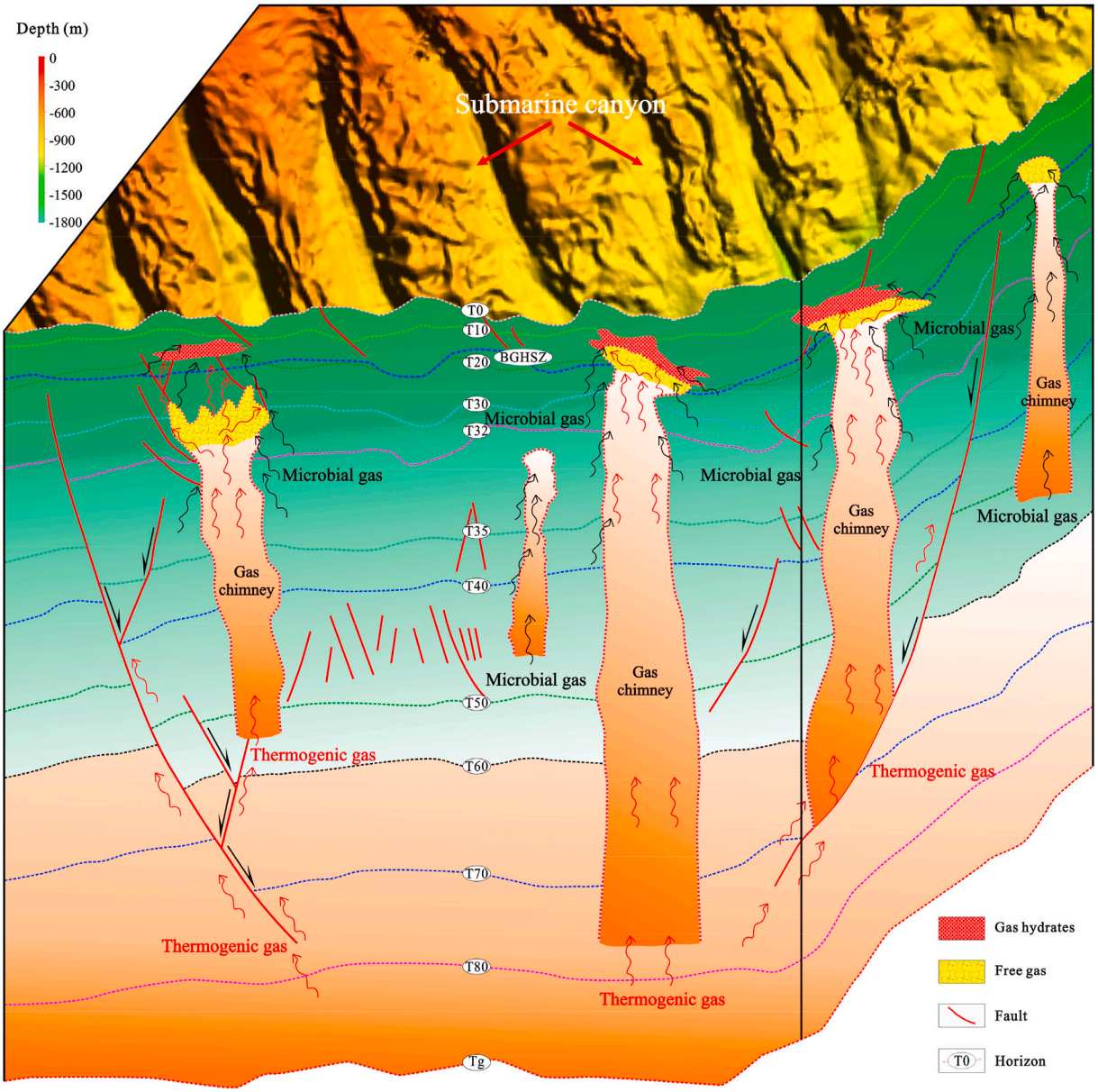


**Fig. 13.** Gas hydrate accumulation model in the Shenhu area. The deep thermogenic gas could be vertically transported into the shallow gas hydrate reservoirs through gas chimneys and faults. Furthermore, in situ microbial gas could also be transported into the GHSZ through the gas chimneys. Additionally, microbial gas in the Yuehai and Wanshan formations may have directly migrated into the GHSZ and formed gas hydrates. Horizons can be seen in Fig. 2. BGHSZ: Base of the gas hydrate stability zone.

reflections can be seen in Fig. 12C and D, resistivity logging showed no obvious anomalies, and no distinct gas migration pathways had been developed at W25 in the seismic data. Gas hydrates of thermogenic origins may not accumulate without apparent gas migration pathways. This was confirmed by the absence of apparent gas migration pathways and resistivity anomalies for W25.

By analyzing the relationship between the drillings, gas hydrate occurrence, and gas chimneys (Table 2), it was determined that a gas

chimney was the most critical factor for gas hydrate accumulation. Gas chimney originated in deep Paleogene source rocks and terminated in shallow Quaternary strata performed a vital role in the formation of thick hydrate layers. Gas chimneys originated in deep formations, which not only effectively connected abundant hydrocarbon gas in source rocks, but also enabled them to pierce into the Quaternary strata (gas hydrate reservoir). They could directly transport the deep hydrocarbon gas upward into the GHSZ because of the overpressure formed by the large number of hydrocarbon fluids that had accumulated within the very thick source rocks.

While gas chimneys originated from shallow formations were difficult to form thick hydrate layers due to the insufficient gas supply, it was less likely for gas hydrates to be formed without gas chimneys as migration pathways.

### 5.3. Gas hydrate accumulation in the shenhu area

On the basis of the analyses of logging and seismic data, the accumulation model of gas hydrate in the Shenhu area was proposed (Fig. 13). The accumulation of hydrocarbons in source rocks resulted in overpressure, and then the Dongsha event might trigger the release of overpressure since the Late Miocene. The gas chimneys formed by the release of overpressure fluids were the primary transporting pathways in the study area. Deep thermogenic gas could have been vertically transported into the shallow gas hydrate reservoirs through faults and gas chimneys. Also, in situ microbial gas could have been transported into the GHSZ through the gas chimneys. Then, at the top of the gas chimneys, free gas had accumulated and showed HRZs on the seismic profiles with the gas hydrates located above.

Although most previous studies showed that the gas source in the Shenhu area was partly of microbial dominance (Liu et al., 2015; Zhu et al., 2013), recent studies have revealed that thermogenic gas was an essential and indispensable gas source and needed to be further studied (Li et al., 2019; Qian et al., 2018; Wei et al., 2018; Zhang et al., 2017).

## 6. Conclusion

Integration between seismic and logging data analyses indicated that the gas chimneys were the key gas migration pathways in the Shenhu area. They were strictly related to the gas hydrate accumulation. Among them, four types of gas chimneys with various top shapes were identified. Furthermore, comprehensive analyses of regional geology, hydrocarbon generation, and tectono-sedimentary evolution in the Baiyun Sag showed that the evolution of gas chimneys could be divided into five stages in terms of the principal factors of overpressure. Based on the integrated well-to-seismic interpretation, gas chimneys were suggested to have been the key gas migration pathways. Also, the deeper the origin of the gas chimney, the shallower the terminal strata at the top, and the more likelihood for the formation of a thick hydrate layer on or above its top. Moreover, the gas hydrate accumulation model in the Shenhu area was mainly derived from the deep thermogenic gas. Then, it was transported upward into the GHSZ through gas chimneys to form gas hydrates.

## Credit author statement

Cong Cheng: Conceptualization, Methodology, Writing - original draft. Tao Jiang: Project administration, Supervision, Investigation, Writing - review & editing, Funding acquisition. Zenggui Kuang: Resources, Investigation, Funding acquisition. Chengzhi Yang: Resources, Formal analysis, Funding acquisition. Cheng Zhang: Investigation, Supervision, Formal analysis. Yunlong He: Investigation, Supervision, Formal analysis. Zhen Cheng: Investigation, Formal analysis. Dongmei Tian: Investigation, Formal analysis. Pengfei Xiong: Investigation, Formal analysis.

## Declaration of competing interest

The authors declare that they have no known competing financial interests or personal relationships that could have appeared to influence the work reported in this paper.

## Acknowledgment

We are very grateful to the Guangzhou Marine Geological Survey for providing logging and seismic data. This work is sponsored by the National Natural Science Foundation of China (No. 41976073), the China Geological Survey Project (No. DD20190230), and the Key Special Project for Introduced Talents Team of Southern Marine Science and Engineering Guangdong Laboratory (Guangzhou) (No. GML2019ZD0102). Moreover, we would like to sincerely thank the journal editor and all anonymous reviewers for their helpful suggestions and constructive comments.

## References

Anderson, B.J., Kurihara, M., White, M.D., Moridis, G.J., Wilson, S.J., Pooladi-Darvish, M., Gaddipati, M., Masuda, Y., Collett, T.S., Hunter, R.B., Narita, H., Rose, K., Boswell, R., 2011. Regional long-term production modeling from a single well test, mount elbert gas hydrate stratigraphic test well, Alaska North Slope. Mar. Petrol. Geol. 28 (2), 493–501.

Audet, D., McConnell, J., 1992. Forward modelling of porosity and pore pressure evolution in sedimentary basins. Basin Res. 4 (2), 147–162.

Bahorich, M.S., Lopez, J., Haskell, N.L., Nissen, S.E., Poole, A., 1995. Stratigraphic and Structural Interpretation with 3-D Coherence, SEG Technical Program Expanded Abstracts 1995. SEG Technical Program Expanded Abstracts. Society of Exploration Geophysicists, pp. 97–100.

Beaudoin, Y., Waite, W., Boswell, R., Dallimore, S., 2014. Frozen Heat: A UNEP Global Outlook on Methane Gas Hydrates, vol. 2. United Nations Environment Programme, Kirkland Trykkery A/S, Norway, p. 77.

Behrens, E.W., 1984. Unifite muds in intraslope basins, northwest Gulf of Mexico. Geo Mar. Lett. 4 (3–4), 227–233.

Boswell, R., Collett, T.S., 2011. Current perspectives on gas hydrate resources. Energy Environ. Sci. 4 (4), 1206–1215.

Boswell, R., Shipp, C., Reichel, T., Shelander, D., Saeki, T., Frye, M., Shedd, W., Collett, T.S., McConnell, D.R., 2016. Prospecting for marine gas hydrate resources. Interpret 4 (1), SA13–SA24.

Cartwright, J., Huuse, M., Aplin, A., 2007. Seal bypass systems. AAPG Bull. 91 (8), 1141–1166.

Chen, D., Wu, S., Dong, D., Mi, L., Fu, S., Shi, H., 2013. Focused fluid flow in the Baiyun Sag, northern South China Sea: implications for the source of gas in hydrate reservoirs. Chin. J. Oceanol. Limnol. 31 (1), 178–189.

Choi, J., Kim, J.-H., Torres, M.E., Hong, W.-L., Lee, J.-W., Yi, B.Y., Bahk, J.-J., Lee, K.E., 2013. Gas origin and migration in the ulleung basin, east sea: results from the second ulleung basin gas hydrate drilling expedition (UBGH2). Mar. Petrol. Geol. 47 (47), 113–124.

Chong, Z.R., Yang, S.H.B., Babu, P., Linga, P., Li, X.-S., 2016. Review of natural gas hydrates as an energy resource: prospects and challenges. Appl. Energy 162, 1633–1652.

Chopra, S., 2002. Coherence cube and beyond. First Break 20 (1), 27–33.

Collett, T.S., 1993. Natural gas hydrates of the Prudhoe Bay and Kuparuk River area, north slope, Alaska. AAPG Bull. 77 (5), 793–812.

Collett, T.S., 2002. Energy resource potential of natural gas hydrates. AAPG Bull. 86 (11), 1971–1992.

Collett, T.S., Agena, W.F., Lee, M.W., Zyrianova, M.V., Bird, K.J., Charpentier, R.R., Cook, T., Houseknecht, D.W., Klett, T.R., Pollastro, R.M., Schenk, C.J., 2008. 2008. Assessment of Gas Hydrate Resources on the North Slope, pp. 2008–3073. Alaska.

Collett, T.S., Johnson, A., Knapp, C.C., Boswell, R., 2009. Natural gas hydrates: a review. In: Collett, T., Johnson, A., Knapp, C., Boswell, R. (Eds.), Natural Gas Hydrates—Energy Resource Potential and Associated Geologic Hazards: AAPG Memoir 89, pp. 146–219.

Coren, F., Volpi, V., Tinivella, U., 2001. Gas hydrate physical properties imaging by multi-attribute analysis—blake Ridge BSR case history. Mar. Geol. 178 (1–4), 197–210.

Fang, H., Xu, M., Lin, Z., Zhong, Q., Bai, D., Liu, J., Pei, F., He, M., 2017. Geophysical characteristics of gas hydrate in the Muli area, Qinghai province. J. Nat. Gas Sci. Eng. 37, 539–550.

Guo, X., Liu, K., He, S., Yang, Z., Dong, T., 2016. Quantitative estimation of overpressure caused by gas generation and application to the Baiyun depression in the Pearl River Mouth Basin, south China sea. Geofluids 16 (1), 129–148.

Haines, S.S., Hart, P.E., Collett, T.S., Shedd, W., Frye, M., Weimer, P., Boswell, R., 2017. High-resolution seismic characterization of the gas and gas hydrate system at Green Canyon 955, Gulf of Mexico, USA. Mar. Petrol. Geol. 82, 220–237.

Hamamoto, H., Yamano, M., Goto, S., Kinoshita, M., Fujino, K., Wang, K., 2011. Heat flow distribution and thermal structure of the Nankai subduction zone off the Kii Peninsula. Geochem. Geophys. Geosyst. 12 (10), 1–22.

He, M., et al., 2017. Rapid post-rift tectonic subsidence events in the Pearl River Mouth Basin, northern South China sea margin. J. Asian Earth Sci. 147, 271–283.
Hsu, H.-H., Liu, C.-S., Chang, Y.-T., Chang, J.-H., Ko, C.-C., Chiu, S.-D., Chen, S.-C., 2017. Diapiric activities and intraslope basin development offshore of SW Taiwan: a case study of the Lower Fangliao Basin gas hydrate prospect. J. Asian Earth Sci. 149, 145–159.
Huang, K., Zhong, G., He, M., Liu, L., Wu, Z., Liu, X., 2018. Growth and linkage of a complex oblique-slip fault zone in the Pearl River Mouth Basin, northern South China sea. J. Struct. Geol. 117, 27–43.
Hunter, R.B., Collett, T.S., Boswell, R., Anderson, B.J., Digert, S.A., Pospisil, G., Baker, R., Weeks, M., 2011. Mount elbert gas hydrate stratigraphic test well, Alaska North Slope: overview of scientific and technical program. Mar. Petrol. Geol. 28 (2), 295–310.
Hutchinson, D.R., Hart, P.E., Ruppel, C.D., Snyder, F., Dugan, B., 2009. Seismic and thermal characterization of a bottom-simulating reflection in the northern Gulf of Mexico. In: Collett, T., Johnson, A., Knapp, C., Boswell, R. (Eds.), Natural Gas Hydrates—Energy Resource Potential and Associated Geologic Hazards: AAPG Memoir 89, pp. 266–286.
Inks, T., Lee, M., Agena, W., Taylor, D., Collett, T., Hunter, M.Z.R., 2009. Seismic prospecting for gas-hydrate and associated free-gas prospects in the Milne Point area of northern Alaska. In: Collett, T., Johnson, A., Knapp, C., Boswell, R. (Eds.), Natural Gas Hydrates—Energy Resource Potential and Associated Geologic Hazards: AAPG Memoir 89, pp. 555–583.
Jia, J., Tsuji, T., Matsuoka, T., 2017. Gas hydrate saturation and distribution in the kumano forearc basin of the Nankai Trough. Explor. Geophys. 48 (2), 137–150.
Jin, J., Wang, X., Guo, Y., Li, J., Li, Y., Zhang, X., Qian, J., Sun, L., 2020. Geological controls on the occurrence of recently formed highly concentrated gas hydrate accumulations in the Shenhu area, South China Sea. Mar. Petrol. Geol. 116, 104294.
Judd, A., Hovland, M., 2009. Seabed Fluid Flow: the Impact on Geology, Biology and the Marine Environment. Cambridge University Press, Cambridge.
Kong, L., Chen, H., Ping, H., Zhai, P., Liu, Y., Zhu, J., 2018. Formation pressure modeling in the Baiyun Sag, northern South China Sea: implications for petroleum exploration in deep-water areas. Mar. Petrol. Geol. 97, 154–168.
Kurihara, M., Ouchi, H., Inoue, T., Yonezawa, T., Masuda, Y., Dallimore, S.R., Collett, T. S., 2005. Analysis of the JAPEX/JNOC/GSC et al. Mallik 5L-38 gas hydrate thermal-production test through numerical simulation. In: Dallimore, S.R., Collett, T.S. (Eds.), Scientific Results from the Mallik 2002 Gas Hydrate Production Research Well Program, Mackenzie Delta, Northwest Territories, Canada, Geological Survey of Canada Bulletin 585.
Kurihara, M., Sato, A., Funatsu, K., Ouchi, H., Yamamoto, K., Numasawa, M., Ebinuma, T., Narita, H., Masuda, Y., Dallimore, S.R., Wright, F., Ashford, D.I., 2010. Analysis of Production Data for 2007/2008 Mallik Gas Hydrate Production Tests in Canada, International Oil and Gas Conference and Exhibition in China. Society of Petroleum Engineers, Beijing, China, p. 24. https://doi:10.2118/132155-MS.
Kvenvolden, K.A., 1993. Gas hydrates-geological perspective and global change. Rev. Geophys. 31 (2), 173–187.
Lei, C., Ren, J., Clift, P.D., Wang, Z., Li, X., Tong, C., 2011. The structure and formation of diapirs in the yinggehai–song hong basin, south China sea. Mar. Petrol. Geol. 28 (5), 980–991.
Li, C.F., Xu, X., Lin, J., Sun, Z., Zhu, J., Yao, Y., Zhao, X., Liu, Q., Kulhanek, D.K., Wang, J., 2014. Ages and magnetic structures of the South China Sea constrained by deep tow magnetic surveys and IODP Expedition 349. Geochem. Geophys. Geosyst. 15 (12), 4958–4983.
Li, J.-f., Ye, J.-l., Qin, X.-w., Qiu, H.-j., Wu, N.-y., Lu, H.-l., Xie, W.-w., Lu, J.-a., Peng, F., Xu, Z.-q., Lu, C., Kuang, Z.-g., Wei, J.-g., Liang, Q.-y., Lu, H.-f., Kou, B.-b., 2018. The first offshore natural gas hydrate production test in South China Sea. China Geol 1 (1), 5–16.
Li, J., Lu, J.a., Kang, D., Ning, F., Lu, H., Kuang, Z., Wang, D., Liu, C., Hu, G., Wang, J., 2019. Lithological characteristics and hydrocarbon gas sources of gas hydrate-bearing sediments in the Shenhu area, South China Sea: implications from the W01B and W02B sites. Mar. Geol. 408, 36–47.
Li, X.-S., Xu, C.-G., Zhang, Y., Ruan, X.-K., Li, G., Wang, Y., 2016. Investigation into gas production from natural gas hydrate: a review. Appl. Energy 172, 286–322.
Liang, J., Wang, H., Su, X., Fu, S., Wang, L., Guo, Y., Chen, F., Shang, J., 2014. Natural gas hydrate formation conditions and the associated controlling factors in the northern slope of the South China Sea. Nat. Gas. Ind. 34 (7), 128–135.
Liang, J., Zhang, Z., Su, P., Sha, Z., Yang, S., 2017. Evaluation of gas hydrate-bearing sediments below the conventional bottom-simulating reflection on the northern slope of the South China Sea. Interpret 5 (3), SM61–SM74.
Liu, C., Meng, Q., He, X., Li, C., Ye, Y., Zhang, G., Liang, J., 2015. Characterization of natural gas hydrate recovered from Pearl River Mouth Basin in south China sea. Mar. Petrol. Geol. 61, 14–21.
Liu, C., Meng, Q., Hu, G., Li, C., Sun, J., He, X., Wu, N., Yang, S., Liang, J., 2017. Characterization of hydrate-bearing sediments recovered from the Shenhu area of the South China Sea. Interpret 5 (3), SM13–SM23.
Majorowicz, J., Osadetz, K., Safanda, J., 2012. Gas hydrate formation and dissipation histories in the northern margin of Canada: beaufort-Mackenzie and the Sverdrup basins. J. Geol. Res. 1–17, 2012.
Majorowicz, J.A., Osadetz, K.G., 2001. Gas hydrate distribution and volume in Canada. AAPG Bull. 85 (7), 1211–1230.
Makogon, Y.F., Holditch, S., Makogon, T.Y., 2007. Natural gas-hydrates—a potential energy source for the 21st Century. J. Petrol. Sci. Eng. 56 (1–3), 14–31.
Merey, Ş., 2016. Drilling of gas hydrate reservoirs. J. Nat. Gas Sci. Eng. 35, 1167–1179.
Mi, L., Zhang, Z., Pang, X., Liu, J., Zhang, B., Zhao, Q., Feng, X., 2018. Main controlling factors of hydrocarbon accumulation in Baiyun Sag at northern continental margin of South China Sea. Petrol. Explor. Dev. 45 (5), 963–973.
Milkov, A.V., 2004. Global estimates of hydrate-bound gas in marine sediments: how much is really out there? Earth Sci. Rev. 66 (3–4), 183–197.
Milkov, A.V., Claypool, G.E., Lee, Y.-J., Sassen, R., 2005. Gas hydrate systems at Hydrate Ridge offshore Oregon inferred from molecular and isotopic properties of hydrate-bound and void gases. Geochem. Cosmochim. Acta 69 (4), 1007–1026.
Miyakawa, A., Saito, S., Yamada, Y., Tomaru, H., Kinoshita, M., Tsuji, T., 2014. Gas hydrate saturation at site C0002, IODP expeditions 314 and 315, in the kumano basin, Nankai Trough. Isl. Arc 23 (2), 142–156.
Pang, X., Chen, C., Peng, D., Zhou, D., Shao, L., He, M., Liu, B., 2008. Basic geology of Baiyun deep-water area in the northern South China Sea. China Offshore Oil Gas 20 (4), 215–222.
Pang, X., Chen, C., Zhu, M., He, M., Shen, J., Lian, S., Wu, X., Shao, L., 2009. Baiyun movement: a significant tectonic event on Oligocene/Miocene boundary in the northern South China Sea and its regional implications. J. Earth Sci. 20 (1), 49–56.
Pang, X., Ren, J., Zheng, J., Liu, J., Yu, P., Liu, B., 2018. Petroleum geology controlled by extensive detachment thinning of continental margin crust: a case study of Baiyun sag in the deep-water area of northern South China Sea. Petrol. Explor. Dev. 45 (1), 29–42.
Peng, C., Zou, C., Lu, Z., Yu, C., Liu, A., Tang, Y., Hu, X., Zhang, S., Wen, H., Li, Y., Wang, W., 2018. Characteristics of gas hydrate reservoirs and their effect on petrophysical properties in the Muli area, Qinghai-Tibetan plateau permafrost. J. Nat. Gas Sci. Eng. 57, 266–283.
Petersen, C.J., Bünz, S., Hustoft, S., Mienert, J., Klaeschen, D., 2010. High-resolution P-Cable 3D seismic imaging of gas chimney structures in gas hydrated sediments of an Arctic sediment drift. Mar. Petrol. Geol. 27 (9), 1981–1994.
Ping, H.W., Chen, H.H., Zhai, P.Q., Zhu, J.Z., George, S.C., 2019. Petroleum charge history in the Baiyun depression and Panyu lower uplift in the Pearl River Mouth Basin, northern South China Sea: constraints from integration of organic geochemical and fluid inclusion data. AAPG Bull. 103 (6), 1401–1442.
Pohlman, J.W., Kaneko, M., Heuer, V.B., Coffin, R.B., Whiticar, M., 2009. Methane sources and production in the northern Cascadia margin gas hydrate system. Earth Planet Sci. Lett. 287 (3), 504–512.
Portnov, A., Santra, M., Cook, A.E., Sawyer, D.E., 2020. The Jackalope gas hydrate system in the northeastern Gulf of Mexico. Mar. Petrol. Geol. 111, 261–278.
Portnov, A., Vadakkepuliyambatta, S., Mienert, J., Hubbard, A., 2016. Ice-sheet-driven methane storage and release in the Arctic. Nat. Commun. 7 (1), 10314.
Qian, J., Wang, X., Collett, T.S., Guo, Y., Kang, D., Jin, J., 2018. Downhole log evidence for the coexistence of structure II gas hydrate and free gas below the bottom simulating reflector in the South China Sea. Mar. Petrol. Geol. 98, 662–674.
Rapoport, A.J., Tjokrosapoetro, S., Charlton, T.R., 1986. Mud volcanoes, shale diapirs, wrench faults, and melanges in accretionary complexes, eastern Indonesia. AAPG Bull. 70 (11), 1729–1741.
Riedel, M., Collett, T.S., Kumar, P., Sathe, A.V., Cook, A., 2010. Seismic imaging of a fractured gas hydrate system in the Krishna–Godavari Basin offshore India. Mar. Petrol. Geol. 27 (7), 1476–1493.
Ruppel, C.D., Kessler, J.D., 2017. The interaction of climate change and methane hydrates. Rev. Geophys. 55 (1), 126–168.
Schofield, N., Jolley, D.W., 2013. Development of intra-basaltic lava-field drainage systems within the Faroe–Shetland Basin. Petrol. Geosci. 19 (3), 273–288.
Shi, H., He, M., Zhang, L., Yu, Q., Pang, X., Zhong, Z., Liu, L., 2014. Hydrocarbon geology, accumulation pattern and the next exploration strategy in the eastern Pearl River Mouth basin. China Offshore Oil Gas 26 (3), 11–22.
Shi, W., Chen, H., Chen, C., Pang, X., Zhu, M., 2007. Pressure evolution and hydrocarbon migration in the Baiyun sag, Pearl River Mouth basin, China. Front. Earth Sci. China 1 (2), 241–250.
Sloan Jr., E.D., Koh, C.A., 2008. Clathrate Hydrates of Natural Gases. CRC press, New York.
Su, M., Sha, Z., Zhang, C., Wang, H., Wu, N., Yang, R., Liang, J., Qiao, S., Cong, X., Liu, J., 2017. Types, characteristics and significances of migrating pathways of gas-bearing fluids in the Shenhu area, northern continental slope of the south China sea. Acta Geol. Sin. -Engl. Ed. 91 (1), 219–231.
Su, M., Yang, R., Wang, H., Sha, Z., Liang, J., Wu, N., Qiao, S., Cong, X., Yang, R., 2016. Gas hydrates distribution in the Shenhu Area, northern South China Sea: comparisons between the eight drilling sites with gas-hydrate petroleum system. Geol. Acta 14 (2), 0079-100.
Su, M., Yang, R., Wu, N., Wang, H., Liang, J., Sha, Z., Cong, X., Qiao, S., 2014. Structural characteristics in the Shenhu Area, northern continental slope of South China Sea, and their influences on gas hydrate. Acta Geol. Sin. -Engl. Ed. 88 (3), 318–326.
Sun, J., Ning, F., Zhang, L., Liu, T., Peng, L., Liu, Z., Li, C., Jiang, G., 2016. Numerical simulation on gas production from hydrate reservoir at the 1st offshore test site in the eastern Nankai Trough. J. Nat. Gas Sci. Eng. 30, 64–76.
Sun, Q., Alves, T., Xie, X., He, J., Li, W., Ni, X., 2017. Free gas accumulations in basal shear zones of mass-transport deposits (Pearl River Mouth Basin, South China Sea): an important geohazard on continental slope basins. Mar. Petrol. Geol. 81, 17–32.
Sun, Q., Wu, S., Cartwright, J., Dong, D., 2012. Shallow gas and focused fluid flow systems in the Pearl River Mouth Basin, northern South China sea. Mar. Geol. 315, 1–14.
Sun, Q., Wu, S., Cartwright, J., Wang, S., Lu, Y., Chen, D., Dong, D., 2014. Neogene igneous intrusions in the northern South China Sea: evidence from high-resolution three dimensional seismic data. Mar. Petrol. Geol. 54, 83–95.
Sun, Z., Zhihong, Z., Di, Z., Xiong, P., Chunju, H., Changmin, C., Min, H., Hehua, X., 2008. Dynamics analysis of the Baiyun sag in the Pearl River Mouth Basin, north of the south China sea. Acta Geol. Sin. -Engl. Ed. 82 (1), 73–83.
Swarbrick, R.E., Osborne, M.J., Yardley, G.S., 2001. Comparision of overpressure magnitude resulting from the main generating mechanisms. In: Huffman, Alan,

Bowers, Glenn (Eds.), Pressure Regimes in Sedimentary Basins and Their Prediction: AAPG Memoir 76, pp. 1–12.
Tian, D., Jiang, T., Liu, B., Liu, J., Zhang, Z., Xu, H., Cheng, C., 2019. Early Miocene sedimentary processes and their hydrocarbon implications in the Baiyun Sag of Pearl River Mouth Basin, northern south China sea. Mar. Petrol. Geol. 101, 132–147.
Trusheim, F., 1960. Mechanism of salt migration in northern Germany. AAPG Bull. 44 (9), 1519–1540.
Van Rensbergen, P., Morley, C., Ang, D., Hoan, T., Lam, N., 1999. Structural evolution of shale diapirs from reactive rise to mud volcanism: 3D seismic data from the Baram delta, offshore Brunei Darussalam. J. Geol. Soc. 156 (3), 633–650.
Wan, Z., Xu, X., Wang, X., Xia, B., Sun, Y., 2017. Geothermal analysis of boreholes in the Shenhu gas hydrate drilling area, northern South China Sea: influence of mud diapirs on hydrate occurrence. J. Petrol. Sci. Eng. 158, 424–432.
Wang, J., Pang, X., Wang, C., He, M., Lian, S.-Y., 2006. Discovery and recognition of the central diapiric zone in Baiyun depression, Pearl River Mouth Basin. Earth Sci. 31 (2), 209–213.
Wang, X., Collett, T.S., Lee, M.W., Yang, S., Guo, Y., Wu, S., 2014a. Geological controls on the occurrence of gas hydrate from core, downhole log, and seismic data in the Shenhu area, South China Sea. Mar. Geol. 357, 272–292.
Wang, X., Hutchinson, D.R., Wu, S., Yang, S., Guo, Y., 2011. Elevated gas hydrate saturation within silt and silty clay sediments in the Shenhu area, South China Sea. J. Geophys. Res.-Solid Earth 116 (B5), 1–18.
Wang, X., Lee, M., Collett, T., Yang, S., Guo, Y., Wu, S., 2014b. Gas hydrate identified in sand-rich inferred sedimentary section using downhole logging and seismic data in Shenhu area, South China Sea. Mar. Petrol. Geol. 51, 298–306.
Wang, Z., He, J., Xie, X., 2004. Heat flow action and its control on natural gas migration and accumulation in mud-fluid diapir areas in Yinggehai basin. Earth Sci. 29 (3), 203–210.
Wang, Z., Huang, B., 2008. Dongfang 1-1 gas field in the mud diapir belt of the Yinggehai Basin, South China Sea. Mar. Petrol. Geol. 25 (4), 445–455.
Wei, J., Fang, Y., Lu, H., Lu, H., Lu, J., Liang, J., Yang, S., 2018. Distribution and characteristics of natural gas hydrates in the Shenhu sea area, south China sea. Mar. Petrol. Geol. 98, 622–628.
Wu, S., Wang, J., 2018. On the China's successful gas production test from marine gas hydrate reservoirs. Chin. Sci. Bull. 63 (1), 2–8 (in Chinese with English abstract).
Xie, H., Zhou, D., Pang, X., Li, Y., Wu, X., Qiu, N., Li, P., Chen, G., 2013. Cenozoic sedimentary evolution of deepwater sags in the Pearl River Mouth Basin, northern South China sea. Mar. Geophys. Res. 34 (3–4), 159–173.
Xie, X., Li, S., Dong, W., Zhang, Q., 1999a. Overpressure development and hydrofracture in the Yinggehai Basin, south China sea. J. Petrol. Geol. 22 (4), 437–454.
Xie, X., Li, S., Hu, X., Dong, W., Zhang, M., 1999b. Conduit system and formation mechanism of heat fluids in diapiric belt of Yinggehai Basin, China. Sci. China Earth Sci. 42 (6), 561–571.
Xie, Z., Sun, L., Pang, X., Zheng, J., Sun, Z., 2017. Origin of the Dongsha event in the south China sea. Mar. Geophys. Res. 38 (4), 357–371.
Yang, J., Wang, X., Jin, J., Li, Y., Li, J., Qian, J., Shi, H., Zhang, G., 2017a. The role of fluid migration in the occurrence of shallow gas and gas hydrates in the south of the Pearl River Mouth Basin, South China Sea. Interpret 5 (3), SM1–SM11.
Yang, R., Su, M., Qiao, S., Cong, X., Su, Z., Liang, J., Wu, N., 2015. Migration of methane associated with gas hydrates of the Shenhu Area, northern slope of South China Sea. Mar. Geophys. Res. 36 (2–3), 253–261.
Yang, S., Lei, Y., Liang, J., Holland, M., Schultheiss, P., Lu, J., Wei, J., 2017b. Concentrated Gas Hydrate in the Shenhu Area, South China Sea: Results from Drilling Expeditions GMGS3 & GMGS4, Proceedings of 9th International Conference on Gas Hydrates, pp. 1–16. Denver, Paper No. 105.
Yang, S., Liang, J., Lei, Y., Gong, Y.H., Xu, H.N., Wang, H.B., Lu, J.A., Holland, M., Schultheiss, P., Wei, J.G., Team, t.G.S., 2017c. GMGS4 gas hydrate drilling expedition in the south China sea. Fire Ice 17 (1), 7–11.
Yang, S., Liang, J., Lu, J.a., Qu, C., Liu, B., 2017d. New understandings on the characteristics and controlling factors of gas hydrate reservoirs in the Shenhu area on the northern slope of the South China Sea. Earth Sci. Front. 24 (4), 1–14.
Zeng, Z., Zhu, H., Yang, X., Zeng, H., Xia, C., Chen, Y., 2019. Using seismic geomorphology and detrital zircon geochronology to constrain provenance evolution and its response of Paleogene Enping Formation in the Baiyun Sag, Pearl River Mouth Basin, South China sea: implications for paleo-Pearl River drainage evolution. J. Petrol. Sci. Eng. 177, 663–680.
Zhang, W., Liang, J., He, J., Cong, X., Su, P., Lin, L., Jin, L., 2018. Differences in natural gas hydrate migration and accumulation between GMGS1 and GMGS3 drilling areas in the Shenhu area, northern South China Sea. Nat. Gas. Ind. 38 (3), 138–148.
Zhang, W., Liang, J., Wei, J., Lu, J.a., Su, P., Lin, L., Huang, W., Guo, Y., Deng, W., Yang, X., Wan, Z., 2020. Geological and geophysical features of and controls on occurrence and accumulation of gas hydrates in the first offshore gas-hydrate production test region in the Shenhu area, Northern South China Sea. Mar. Petrol. Geol. 114, 104191.
Zhang, W., Liang, J., Wei, J., Su, P., Fang, Y., Guo, Y., Yang, S., Zhang, G., 2017. Accumulation features and mechanisms of high saturation natural gas hydrate in Shenhu Area, northern South China Sea. Petrol. Explor. Dev. 44 (5), 708–719.
Zhao, S., Wu, S., Shi, H., Dong, D., Chen, D., Wang, Y., 2012. Structures and dynamic mechanism related to the Dongsha movement at the northern margin of South China Sea. Prog. Geophys. 27 (3), 1008–1019.
Zhao, Y., Ren, J., Pang, X., Yang, L., Zheng, J., 2018. Structural style, formation of low angle normal fault and its controls on the evolution of Baiyun Rift, northern margin of the South China Sea. Mar. Petrol. Geol. 89, 687–700.
Zhong, G., Liang, J., Guo, Y., Kuang, Z., Su, P., Lin, L., 2017. Integrated core-log facies analysis and depositional model of the gas hydrate-bearing sediments in the northeastern continental slope, South China Sea. Mar. Petrol. Geol. 86, 1159–1172.
Zhu, Y., Huang, X., Fu, S., Su, P., 2013. Gas sources of natural gas hydrates in the Shenhu Drilling Area, South China Sea: geochemical evidence and geological analysis. Acta Geol. Sin. -Engl. Ed. 87 (3), 767–776.
Zühlsdorff, L., Spieß, V., 2004. Three-dimensional seismic characterization of a venting site reveals compelling indications of natural hydraulic fracturing. Geology 32 (2), 101–104.